

**Concept and Feasibility Study of Self-Organized  
Electrochemical Devices**

by

William Douglas Moorehead

Bachelor of Science, Chemistry  
United States Naval Academy, May 1996

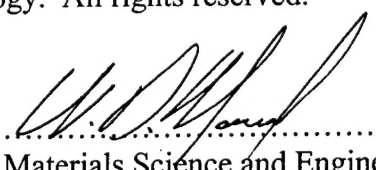
Submitted to the Department of Materials Science and Engineering  
in Partial Fulfillment of the Requirements for the Degree of

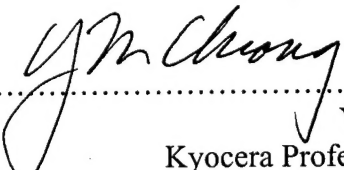
Master of Science in the Department of Materials Science and Engineering  
at the

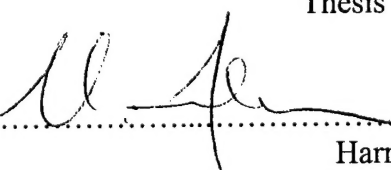
Massachusetts Institute of Technology

September 2002

© 2002 Massachusetts Institute of Technology. All rights reserved.

Signature of Author.....  
Department of Materials Science and Engineering  
July 26, 2002

Certified by.....  
Yet-Ming Chiang  
Kyocera Professor of Ceramics  
Thesis Supervisor

Accepted by.....  
Harry L. Tuller  
Professor of Ceramics and Electronic Materials  
Chair, Departmental Committee on Graduate Students

**DISTRIBUTION STATEMENT A**  
Approved for Public Release  
Distribution Unlimited

20030220 031

AD NUMBER		DATE 05 Feb 03	DTIC ACCESSION NOTICE
1. REPORT IDENTIFYING INFORMATION		REQUESTED.	
A. ORIGINATING AGENCY NAVAL POSTGRADUATE SCHOOL, MONTEREY, CA 93943		1. Put y on re	
B. REPORT TITLE AND/OR NUMBER CONCEPT & FEASIBILITY STUDY OF SELF-ORGANIZED ELECTROCHEMICAL DEVICES		2. Comf	
C. MONITOR REPORT NUMBER BY: WILLIAM D. MOOREHEAD, MIT		3. Attac mail	
D. PREPARED UNDER CONTRACT NUMBER N62271-97-G-0026		4. Use i info.	
2. DISTRIBUTION STATEMENT		5. Do n for i	
APPROVED FOR PUBLIC RELEASE; DISTRIBUTION UNLIMITED		DTIC: 1. Assl 2. Relt	

20030220 031

DTIC Form 50  
DEC 91

PREVIOUS EDITIONS ARE OBSOLETE

# Concept and Feasibility Study of Self-Organized Electrochemical Devices

By

William Douglas Moorehead

Submitted to the Department of Materials Science and Engineering on July 26, 2002  
in Partial Fulfillment of the Requirements for the Degree of  
Master of Science

## ABSTRACT

Since Volta's discovery of "an electric battery" in 1800, advancements have proceeded due to great materials advances. However, the basic configuration he proposed then is still present in today's portable power sources. In this work, using attractive and repulsive London-van der Waals forces, a self-organized, interpenetrating, separator-free rechargeable lithium ion battery called a self-organized battery system (SBS) is proposed. In this design, a repulsive interaction between the cathode and anode is used to establish the basic electrochemical junction. Increases in both energy density (Wh/kg, Wh/l) and power density (W/kg, W/l) are possible from such a design, due to 1) the decrease of inactive materials required, and 2) the decrease in Li ion diffusion length between the cathode and anode.

The sign of the Hamaker constant ( $A_{123}$ ) determines either attraction (+) or repulsion (-) where material 2 is the intervening material between materials 1 and 3. For low refractive index materials ( $n < 2$ ),  $A_{123}$  is determined primarily by the average refractive index of materials 1, 2, and 3 in the visible range. For a repulsive interaction, where  $A_{123} < 0$ , the refractive index of materials 1, 2, and 3 must be  $n_1 < n_2 < n_3$ , or  $n_1 > n_2 > n_3$ .

All close packed oxide cathode structures ( $\text{LiMO}_2$ , where  $M = \text{Mn, Co, Ni}$ ) that are currently used in Li ion technology have refractive indexes  $> 2$ . However, a new class of cathode materials based upon the olivine,  $\text{LiFePO}_4$ , allows  $n_1 < n_2 < n_3$  to be achieved with the use of organic solvents as the intervening medium. Furthermore, low refractive index conductive/insulating polymer blends were studied as a potential coating on  $\text{LiMO}_2$  cathode materials.

Single-wave ellipsometry measurements were taken on doped  $\text{LiFePO}_4$  and the polymer blends in order to determine the refractive index. Electronic isolation between the conductive polymer blend and both MCMB and Mg-doped  $\text{LiCoO}_2$  was achieved as well as between doped  $\text{LiFePO}_4$  and MCMB.

Electrochemical cycling was performed on several SBS cells. Upon electrochemical cell assembly, open circuit voltages were observed. Upon cycling, The cell voltages observed upon intercalation are thermodynamically consistent with the cathode and anode materials present in the systems. Comparisons to conventional cells using Celgard separator between the cathode and anode are made.

Thesis Supervisor: Yet-Ming Chiang

Title: Kyocera Professor of Ceramics, Department of Materials Science and Engineering

## Acknowledgments

First, I would like to acknowledge my friend and advisor, Professor Yet-Ming Chiang, for providing me with such wonderful educational opportunities. No class or seminar series can contribute more to a researcher's development than the close advisor-student relationship that I had with Yet-Ming Chiang, for which I will be always grateful.

I am grateful to the great members of Prof. Chiang's research group for all of their assistance and support. Mrs. Toni Centorino has provided excellent support during my two years of research.

I also want to acknowledge Mr. Mike Frongillo for his assistance and training with TEM and SEM, Mr. Joe Adario for his help with X-ray Diffraction experiments, and Ms. Libby Shaw for her assistance in using the Gaertner Ellipsometer.

I thank my wonderful wife, Mrs. Kevin Elizabeth Moorehead, for providing a constant source of encouragement and humor. I also thank the U.S. Navy for allowing me this time to complete my Master of Science degree.



# Table of Contents

Abstract .....	2
Acknowledgements .....	3
Table of Contents .....	4
List of Figures .....	7
List of Tables .....	10
CHAPTER 1. Overview of Current Li Ion Battery Technology .....	11
1.1. Secondary Lithium Ion Batteries .....	11
1.2. Cathode and Anode Materials of Interest .....	14
1.3. Current Status of Battery Electrolytes .....	15
1.4. Summary .....	17
1.5. References .....	18
CHAPTER 2. Using London Dispersion Forces for High Energy Density, High Power Density, Self-organized Batteries .....	19
2.1. London Dispersion Forces .....	20
2.2. Calculation of the Hamaker Constant .....	22
2.3. Self-Organized Batteries Using van der Waals Forces .....	22
2.4. SBS Comparison with Conventional Cylindrical Cells: Performance Gains from the Interpenetrating Design .....	24
2.5. References .....	26
CHAPTER 3. Electronically Conductive Polymer Blends and Their Application .....	27
3.1. Introduction .....	27
3.2. POMA/PVdF Conductive Blends .....	29
3.2.1. Introduction .....	29
3.2.2. Synthesis of Conductive Polymer Blends .....	31
3.3. Conductivity Measurements of Polymer Blends .....	31
3.3.1. Experimental .....	31
3.3.2. Observations .....	32
3.3.3. Conclusions .....	32

3.4.	Refractive Index Measurement of 10 WT% POMA/90 WT% PVdF	
	Conductive Blend .....	33
3.4.1.	Experimental .....	33
3.4.2.	Observations .....	33
3.4.3.	Conclusions .....	35
3.5.	Coating of Particles with a 10 WT% POMA/90 WT% PVdF Conductive Blend.....	35
3.6.	Summary .....	35
3.7.	References.....	36
CHAPTER 4.	Electronic Isolation Experiments.....	37
4.1.	Layered POMA/PVdF-PEO/DIM-MCMB Isolation Experiment.....	38
4.1.1.	Experimental.....	38
4.1.2.	Observations .....	39
4.1.3.	Conclusions .....	42
4.2.	Layered Ag-POMA/PAN-PEO/DIM-LMCO Experiment.....	42
4.2.1.	Motivation for a POMA/PAN Polymer Blend .....	42
4.2.2.	Experimental.....	42
4.2.3.	Observations .....	43
4.2.4.	Conclusions .....	45
4.3.	Layered LMCO-PS/DIM-POMA/PVdF Isolation Experiment.....	45
4.3.1.	Experimental.....	45
4.3.2.	Observations .....	46
4.3.3.	Conclusions .....	47
4.4.	Isolations Experiments Using LiFePO <sub>4</sub> .....	47
4.4.1.	Experimental.....	48
4.4.2.	Observations .....	49
4.4.3.	Conclusions .....	49
4.5.	Isolations Experiments Substituting 1,2-diiodoethane (DIE) for diiodomethane.....	50
4.5.1.	Experimental.....	50
4.5.2.	Observations .....	51

4.5.3. Conclusions .....	51
4.6. Cell Preparation and Cycling Experiments .....	52
4.7. Conclusions of Electronic Isolation Experiments .....	57
4.8. References.....	58
CHAPTER 5. Self-Organized Cells Using Colloidal Particle Cathode and Anodes.....	59
5.1. MCMB-PS/DIM-Conductive LFP Printed onto POMA/PVdF Substrates ....	59
5.1.1. Experimental.....	60
5.1.2. Observations .....	63
5.1.3. Discussion.....	66
5.2. Self-Organized MCMB-PS/DIM-Conductive LFP on POMA/PVdF Substrates, Cycled in a Pressure Free Cell .....	67
5.2.1. Experimental.....	67
5.2.2. Observations .....	70
5.2.3. Conclusions .....	72
5.3. Self-Organized MCMB-PS/DIM-Conductive LFP Suspensions on POMA/PVdF Substrates: Effect of PS Fraction and Phase Purity of LFP Powder .....	72
5.3.1. Experimental.....	72
5.3.2. Observations .....	73
5.3.3. Conclusions .....	75
CHAPTER 6. Conclusions.....	76

# List of Figures

Figure 1.1	Illustration of Conventional Li Ion Battery. ....	12
Figure 1.2	The electrochemical potential of the anode reductant and the cathode oxidatant must lie between the electrolyte energy gap ( $E_g$ ). Thermodynamically, $\mu_A - \mu_C \leq E_g$ .....	13
Figure 2.1	Dispersion for self-organized battery system (SBS). ....	20
Figure 2.2	wt% and vol% distribution of materials in conventional Li ion cells.....	24
Figure 3.1	Illustration of low refractive index, electronically conductive polymer coating on the cathode in order to give $A_{123} < 0$ .....	28
Figure 3.2	10 wt% POMA/90 wt% PVdF dimensions with Ag paint leads on the ends for electronic conductivity measurements. The film was cast onto a glass substrate .....	32
Figure 3.3	a) SEM analysis of 10 wt% POMA/90 wt% PVDF (TFA doped) .....	34
Figure 3.3	b) SEM analysis of 10 wt% POMA/90 wt% PVDF (TFA doped) .....	34
Figure 4.1	Experiment demonstrating electronically insulating junctions between two conductive materials in a system expected to have a negative Hamaker constant. Cross-section SEM analysis shows the PEO wetting between the MCMB and the conductive polymer blend as expected for $A_{123} < 0$ , where 1 is the conductive polymer blend, 2 is the DIM, and 3 is the MCMB .....	39
Figure 4.2	Experimental configuration for measuring resistance across each conductive film and between the two films.....	40
Figure 4.3	Schematic of the through layer resistance measurement showing electronic isolation between LMCO and POMA/PAN .....	44

Figure 4.4	Schematic of layered assembly for cycle testing. ....	46
Figure 4.5	Voltage vs. capacity for layered cell Ag-POMA/PVDF-PS/DIM-LMCO. The current rate and the capacity is calculated for the LMCO mass .....	47
Figure 4.6	Layered configuration where it is expected that the condition $A_{123} > 0$ will exist between the MCMB and the LFP. ....	48
Figure 4.7	Schematic of sample for electrochemical testing .....	51
Figure 4.8	Sample preparation for electrochemical testing.....	52
Figure 4.9	Charge curve for cell of the configuration illustrated in Figure 4.8, tested at 25°C. The current rate and the capacity is calculated for LFP mass .....	53
Figure 4.10	Charge curve for cell of the configuration illustrated in Figure 4.8, tested at 50°C. The current rate and the capacity is calculated for LFP mass .....	54
Figure 4.11	Cycling of undoped $\text{LiFePO}_4$ vs. Li in a stainless steel screw-top electrochemical cell using Celgard separator. 10 wt% PVdF was used as a binder in the cathode. No carbon additive was used.....	55
Figure 4.12	Four charge/discharge cycles for cell of the configuration illustrated in Figure 4.8, tested at 50°C. The current rate and the capacity is calculated for LFP mass .....	56
Figure 4.13	OCV measurements for a cell after charging to 3.8 volts.....	57
Figure 5.1	Cell configuration of full SBS cells using 50 vol% active material $\{\text{Li}(\text{Zr}_{0.02}\text{Fe}_{0.98})\text{PO}_4$ and MCMB}/50 vol% PS (50,000 M.W.) cast onto POMA/PVDF substrates.....	59
Figure 5.2	a) Digital photograph of cell upon removal from vacuum at room temperature before transfer to argon filled glovebox. ....	61

Figure 5.2	b) Digital photograph of cells upon removal from vacuum at room temperature before transfer to argon filled glovebox .....	62
Figure 5.3	Charge/discharge curves for 4 cycles, with an upper voltage cut-off of 4.5 V and lower cut-off of 2.5 V (Cell PS 210).....	63
Figure 5.4	Expanded view of the capacity curve around 20 mAh/g of Figure 5.3.....	64
Figure 5.5	Monitoring OCV of SBS cell (Cell PS 210).....	65
Figure 5.6	Second cycling of SBS cell (Cell PS 210) .....	65
Figure 5.7	Pressure-free electrochemical cell assembly .....	69
Figure 5.8	Charging of SBS cell with pressure-free configuration (PS 215).....	70
Figure 5.9	OCV of SBS cell PS 215, showing that an OCV of 3.6 V is held for over 20 hours.....	71
Figure 5.10	Charge data of cell PS215 after holding 3.6 volts for over 20 hours.....	71
Figure 5.11	$\text{LiTi}_{0.02}\text{Fe}_{0.98}\text{PO}_4$ cycled against MCMB in a self-organized system (Cell PS 233).....	74
Figure 5.12	Data collected 7 hours after first data set collected (Figure 5.11). First charge shows a capacity of only 8 mAh/g compared to 80 mAh/g in the first charge curve of Figure 5.11 (Cell PS 233).....	75

## List of Tables

Table 1.1	Performance comparison of Lead acid, NiMH, and Li Ion cells.....	11
Table 1.2	Representative anode material classes with their associated safety and performance concerns. ....	15
Table 3.1	Summary of conductive polymers available.....	29
Table 4.1	Resistance measurements recorded between films of POMA/PVdF and 60 vol% MCMB/40 vol% PEO. The separation distance between the two probes corresponds to the measurement points referenced in Figure 4.2. Points A, G, and E correspond to the POMA/PVdF film and points B, C, D, and F correspond to the MCMB/PEO film.....	41

## CHAPTER 1. Overview of Current Li Ion Battery Technology

### 1.1 Secondary Lithium Ion Batteries

In 1800, Volta described two constructions for batteries. One, termed “the pile,” consisted of alternate discs of Zn and Cu separated by pieces of wet pasteboard. The other, the crown of cups, had series connected cells in separate cups using two dissimilar metals placed on opposite sides of each cup filled with electrolyte [1-1]. Since Volta’s discovery, several sciences within the battery field have developed. Table 1.1 gives a performance overview of lead acid (PbA), nickel-metal hydride (NiMH), and Li ion battery systems [1-2].

	PbA	NiMH	Li Ion
Wh/kg	20-40	40-80	80-170
Wh/l	40-80	150-300	300-450
\$/kWh	150-300	600	600
W/kg	100-300	400-800	800-2000
W/l	200-600	1000-2000	2000-5000
\$/kW	10-20	50	30

**Table 1.1** Performance comparison of Lead acid, NiMH, and Li Ion cells

As seen in Table 1.1, Li ion battery systems receive a great deal of attention as they provide greater energy density (Wh/kg, Wh/l) and greater power density (W/kg, W/l) compared to NiMH and PbA.



Current lithium rechargeable battery technology first appeared in 1990 when Sony abandoned their Li/MnO<sub>2</sub> rechargeable battery to introduce a new concept, which they named Li Ion [1-3]. Since then, considerable research has been carried out worldwide on lithiated cathode materials and suitable lithium host anode materials. Figure 1.1 shows

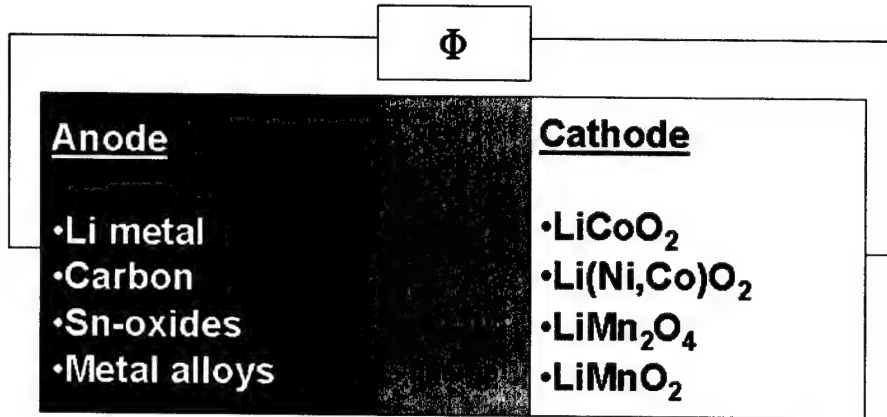


**Figure 1.1** Illustration of Conventional Li Ion Battery

a conventional Li Ion cell configuration. Upon charging, Li ions are removed from the cathode where oxidation occurs and travel through the electrolyte to intercalate into the anode. Electrons travel through the external loop to the anode. Once charged, the chemical potential of Li at the anode is greater than at the cathode and a cell voltage develops, which is directly proportional to the Li chemical potential difference between the anode and cathode according to the following equation [1-4]:

$$OCV = V(x) = - \frac{\mu_{Li}^{cathode}(x) - \mu_{Li}^{anode}(x)}{zF} = - \frac{RT}{F} \cdot \ln \frac{a_{Li}^{cathode}}{a_{Li}^{anode}}$$

A high chemical potential difference between anode and cathode is desirable in order to achieve a high cell voltage, which can lead to increased energy density (Wh/kg); a measure of the energy storage capacity. The energy density of a battery is a product of

the specific capacity (Ah/kg) and the average intercalation voltage. However, practical voltages of Li Ion cells are limited by the fact that the attainable difference ( $\mu_A - \mu_C$ ) must be less than the energy gap ( $E_g$ ) between the HOMO and the LUMO of the liquid electrolyte (Figure 1.2).

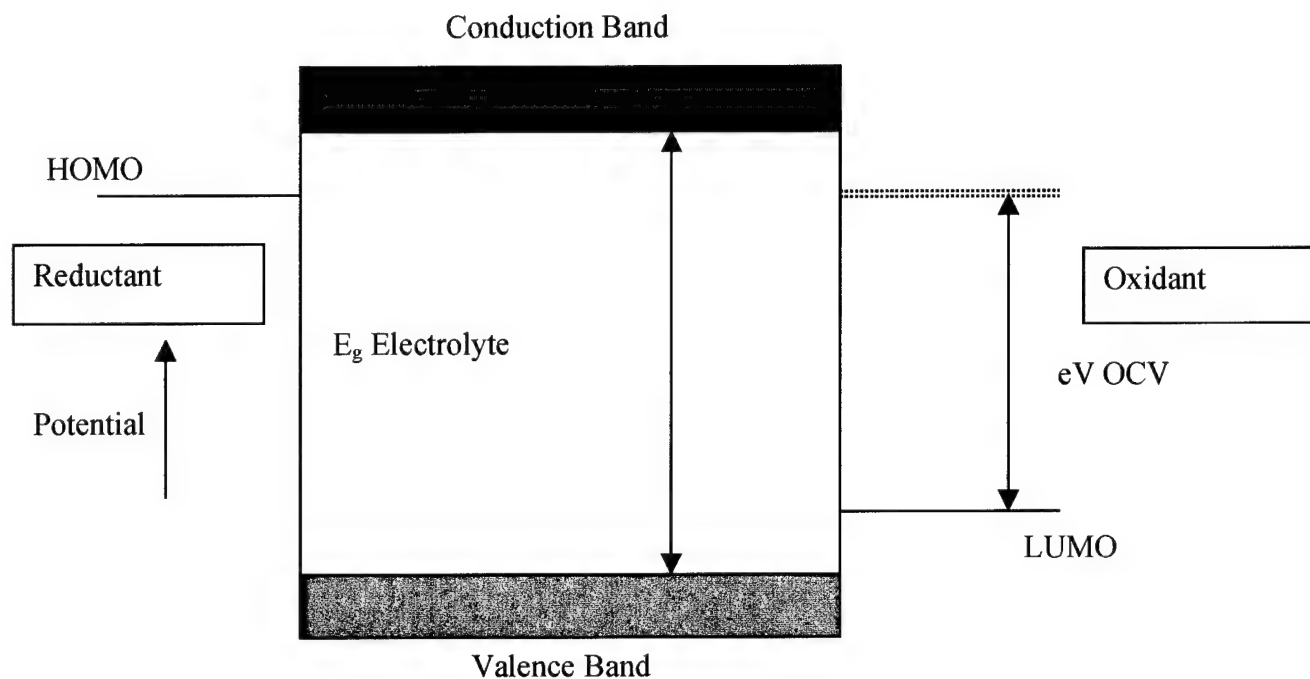


**Figure 1.2** The electrochemical potential of the anode reductant and the cathode oxidant must lie between the electrolyte energy gap ( $E_g$ ). Thermodynamically,  $\mu_A - \mu_C \leq E_g$ .

One measure of the quality of an electrolyte is its transference (or transport) number

$$t_i \equiv \sigma_i / \sigma$$

where  $\sigma$  is the sum of all the ionic conductivities and the electronic conductivity ( $\sigma_e$ ) of the electrolyte under the working conditions of the cell. An ideal electrolyte has  $t_i=1$ . If liquid electrolyte is used, a separator is needed to maintain an even spacing between the

electrodes while blocking electronic current and passing ionic current. Common separators are porous electronic insulators permeated by a single liquid electrolyte.

## **1.2 Cathode and Anode Materials of Interest**

Since AEA's discovery of  $\text{LiCoO}_2$  and  $\text{LiNiO}_2$  in 1979, they have served as some of the primary cathode materials along with spinel  $\text{LiMn}_2\text{O}_4$ , which was discovered later [1-5]. However,  $\text{LiCoO}_2$  is reactive with the liquid electrolyte in the charged state, with cell explosions having been documented over the years when  $\text{LiCoO}_2$  is used as the cathode. Furthermore, Co is expensive, with an average 10 year price of \$20.87/pound. These facts have constrained the application of  $\text{LiCoO}_2$ -based cells to small applications such as cell phones and laptops [1-6]. For  $\text{LiMn}_2\text{O}_4$ , a high rate capability is obtainable along with low material costs; however, the spinel  $\text{LiMn}_2\text{O}_4$  has a low practical capacity of 110 mAh/g. More recent,  $\text{LiNi}_{1-x}\text{M}_x\text{O}_2$  has been synthesized (where  $\text{M}=\text{Mn, Ti}$ ) with good stability and high capacity of 200 mAh/g [1-7]. Another promising new cathode is  $\text{Li}_x\text{Mn}_{0.4}\text{Ni}_{0.4}\text{Co}_{0.2}\text{O}_2$ , which shows reversible capacity of 180 mAh/g [1-8]. While continued development of new cathodes is expected, the rate of increase in energy density is likely to be modest.

The inherent dangers of using metallic lithium as an anode resulted in extensive research for a suitable replacement. In 1981, Sanyo developed graphite for use as a lithium battery anode, which delivers a capacity of 372 mAh/g [1-5]. Numerous other families of materials have been studied as potential replacements of higher energy density. Table 1.2 gives a comparison of some alternative anode materials for lithium ion batteries.

Anode Material	Issues
Alloys (i.e. $\text{Li}_x\text{Sn}$ , $\text{Li}_x\text{Al}$ , $\text{Li}_x\text{Si}$ )	swelling, pulverization of particles, loss of capacity with cycling
Compounds (i.e. $\text{Li}_x\text{TiS}_2$ , $\text{LiTiO}_2$ , $\text{LiSnO}_y$ )	irreversibility, swelling, usable only with delithiated cathodes
Li Metal	dendritic growth, low coulombic efficiency

**Table 1.2** Representative anode material classes with their associated safety and performance concerns.

As an example of a new anode under study,  $\text{Li}_3\text{N}$  has a large bandgap and very low electronic conductivity. However,  $\text{Li}_{3-x}\text{Co}_x\text{N}$  is electronically conductive with a conductivity value similar to that of  $\text{LiCoO}_2$  of  $10^{-3}$  S/cm. Specifically,  $\text{Li}_{2.6}\text{Co}_{0.4}\text{N}$  provides a capacity of 600 mAh/g, with only a 0.02% capacity fade per cycle. The average potential of  $\text{Li}_{3-x}\text{Co}_x\text{N}$  vs. Li is 0.7-0.8 V [1-9].  $\text{Li}_{3-x}\text{Co}_x\text{N}$  is processed in the crystalline state, but becomes completely amorphous during the first discharge and remains so during subsequent discharges. With a relatively high potential with respect to lithium,  $\text{Li}^+$  is able to be reversibly exchanged without the plating of lithium on the anode. However, for  $\text{Li}_{3-x}\text{Co}_x\text{N}$  to be used in a practical Li ion cell, the cathode has to be in a delithiated state upon assembly.

### 1.3 Current Status of Battery Electrolytes

Essentially all room temperature Li ion batteries use an organic liquid electrolyte with lithium ion conductivities around  $10^{-2}$  S/cm. For decades, researchers have worked to replace the liquid electrolyte with a solvent free, Li salt doped, polymer based system. The driving force for a solid polymer electrolyte (SPE) is high, as the lightweight polymer could serve as both the electrolyte and the physical separator. Nearly all polymer electrolytes use a poly(ethylene oxide) (PEO) based system that provides the

conduction mechanism for  $\text{Li}^+$  ions. However, all dry polymer electrolytes still give a room temperature conductivity of at most  $10^{-4}$  S/cm. In the current conventional layered battery configuration, the average diffusion length of Li can be as high as 100 microns. Such a low ionic conductivity value for  $\text{Li}^+$  is insufficient to allow for reasonable battery performance using SPE's at room temperature.

With respect to liquid electrolytes, which are solutions of lithium salts in aprotic organic solvents, systematic research on different additives and organic solvent combinations has been conducted in order to increase the operating capabilities of current batteries. One example of a typical electrolyte is 1:1:1 ethylene carbonate (EC): dimethyl carbonate (DMC): ethylmethyl carbonate (EMC) mixture, which is suitable to  $-20^\circ\text{C}$ . Cathodes and anodes allowing 5 volt batteries do exist; however, conventional organic liquid electrolytes are oxidized at voltages generally in excess of 4.3 volts. Ultimately, the LUMO of the electrolyte components indicates the reduction potential. Additives to the electrolyte solution suppress electrolyte decomposition, increase the level of flame retardance, improve wettability, add overcharge/overdischarge protection, and improve high temperature performance. Furthermore, much research has been conducted to replace the most commonly used Li salt,  $\text{LiPF}_6$ , due to its reaction with  $\text{H}_2\text{O}$  and subsequent formation of HF, which chemically reacts with other battery components and can be a source of failure.

## 1.4 Summary

Li ion battery technology is making systematic but incremental strides in performance. Virtually all current cell phones and laptops are powered by lithium battery technology. Researchers continue to boost the energy density and power density of Li ion cells, increase the safety, and improve the environmental friendliness while cutting costs. However, compared to the computing industry, where processing power and transistor density is doubling every 18 months, the lithium battery field has been perceived to be limited by fundamental scientific principles that cannot be overcome simply with enhanced processing.

In this thesis, a fundamental change in battery design that could lead to a revolutionary change in the way batteries are manufactured and used is explored. Based upon London-van der Waals forces, an interpenetrating electrode, separator-free, self-organizing battery design is experimentally studied for rechargeable lithium ion batteries. Such an interpenetrating design can dramatically increase energy density and power density, lower manufacturing costs, and allow batteries to be used in applications not previously considered.

## 1.5 References

- 1-1. D. Georgi, "2000 AD – Two Hundredth Anniversary of Volta's Invention", Battery Digest Newsletter, No. 46, 1-5, (2000)
- 1-2. J. Reimers, "Li Technology for Transportation Applications", Abstract No. 416, IMLB 11, Monterey, CA; June 23-28, 2002.
- 1-3. M. Broussely, P. Biensan, B. Simon, "Lithium insertion into host materials: the key to success for Li ion batteries", *Electrochimica Acta*, **45**, 3 (1999).
- 1-4. G. Pistoia, Lithium Batteries (Elvesier, Amsterdam, 1994).
- 1-5. S. Narukawa et al. "Recent advances in Li-ion Polymer Battery Technology" Abstract No. 2, IMLB 11, Monterey, CA; June 23-28, 2002.
- 1-6. 1988-1998 U.S. spot price, 99.8% cobalt cathode, Platt's Metals Week.
- 1-7. R.J. Brodd, "Status of Rechargeable Lithium Battery Technology", Abstract No. 1, IMLB 11, Monterey, CA; June 23-28, 2002.
- 1-8. 7. S. Whittingham et al. "Layered Cathode Materials", Abstract No. 207, IMLB 11, Monterey, CA; June 23-28, 2002.
- 1-9. Y. Nitta, M. Hasegawa, M. Kayama, "Nitride Negative Electrode of Lithium Battery", Abstract No. 8, IMLB 11, Monterey, CA; June 23-28, 2002.

## **CHAPTER 2. Using London Dispersion Forces for High Energy Density, High Power Density, Self-Organized Batteries.**

Based on the assessment of secondary Li ion battery technology in the first chapter, it is not unreasonable to say that for the last 200 years, we have improved our existing battery technology primarily by improving the individual existing parts; cathode, anode, and electrolyte. However, all technologies to date still use the layered configuration of cathode and anode with a physical separator providing electronic isolation.

Using attractive and repulsive van der Waals forces, the interpenetrating, dispersion force self-organized battery system in Figure 2.1 is proposed. This device design will be referred to as “SBS” henceforth. This design should allow for a separator-free battery with greatly increased loading of the electroactive species (cathode and anode). In Figure 5.1, attractive forces are required between material 1 (cathode particles) and between material 1 and the positive current collector when they are dispersed in a fluid, material 2, in order to have electronic percolation throughout the cathode network. Attractive forces are also required between material 3 (anode particles) and between material 3 and the negative current collector when they are dispersed in material 2, in order to have electronic percolation throughout the anode network. However, for electronic isolation of the cathode and anode, repulsive interactions are required between material 1 (cathode) and material 3 (anode) when they are dispersed in material 2. Furthermore, to avoid shorting between the current collectors, repulsive interactions are also required between material 1 (cathode) and the negative current collector and between material 3 (anode) and the positive current collector when dispersed in material 2.



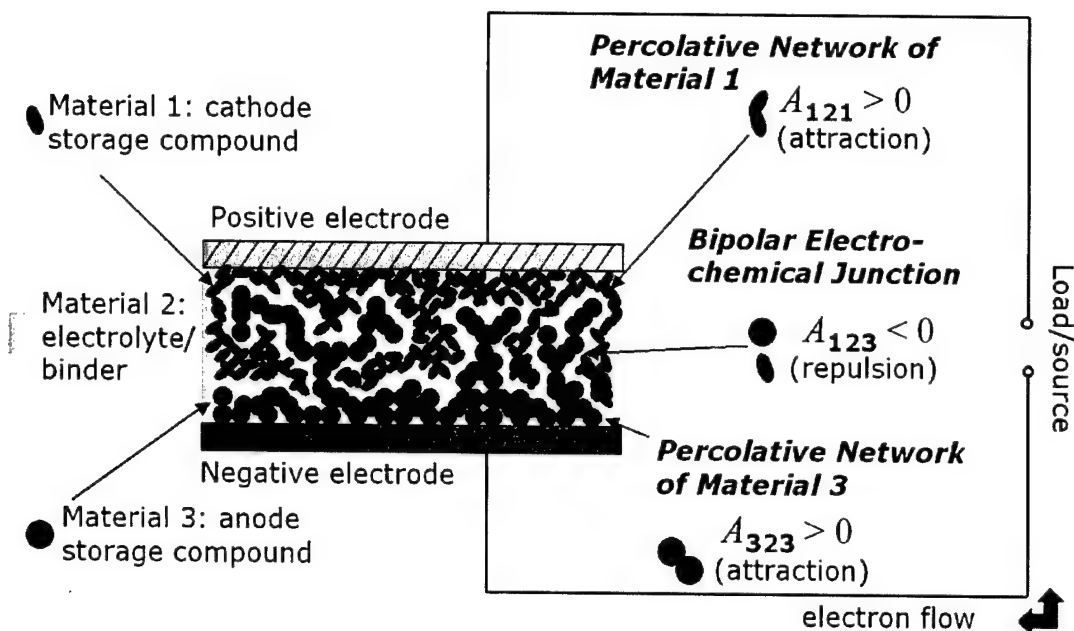


**Figure 2.1** Dispersion force self-organized battery system (SBS).

## 2.1 London Dispersion Forces

The existence of adhesive forces between small particles is well-known. In 1937, H.C. Hamaker attributed the adhesion mainly to London-van der Waals forces and worked to determine the magnitude and range of these forces. Hamaker concluded that the London-van der Waals forces between two particles of the same material embedded in a fluid is always attractive, provided there is no marked orientation of the fluid molecules. If the particles are of different composition, the resulting force may be repulsive [2-1]. Among the many contributions to the interaction between surfaces, e.g. double layer, structural, steric, depletion, hydration and hydrophobic forces, the van der Waals interaction is the only one that is always present.

The van der Waals force has an electrodynamic origin arising from the interactions between atomic or molecular oscillating or rotating electrical dipoles within the interacting media. There are three types of interactions which contribute to the van der Waals Force. First, there is the Keesom force, which is the interaction between

permanent dipoles. Second is the Debye force, which is the interaction between permanent dipoles and induced dipoles. Third, the London or dispersion force is the interaction between induced dipoles [2-2]. Hamaker calculated the distance dependence of the free energy of macroscopic bodies by performing a pair-wise summation over all the atoms in the bodies. Between semi-infinite parallel plates at separation  $L$ , the van der Waals interaction free energy,  $V_{vdW}$ , can be expressed as [2-3]:

$$V_{vdW} = -\frac{A_{123}}{12\pi L^2} \quad \text{Eq. 2.1}$$

The force per unit area is equal to the negative spatial derivative of the energy.

$$F_{vdW} = -\frac{A_{123}}{6\pi L^3} \quad \text{Eq. 2.2}$$

For two spheres with radii  $R_1$  and  $R_2$  and distance of closest approach  $H$ , where  $R_1, R_2 \gg H$ , the van der Waals interaction energy and force can be expressed as [2-3]:

$$V_{vdW} = -\frac{A_{123} R_1 R_3}{6 H (R_1 + R_3)} \quad \text{Eq. 2.3}$$

$$F_{vdW} = -\frac{A_{123} R_1 R_3}{6 H^2 (R_1 + R_3)} \quad \text{Eq. 2.4}$$

where  $A$  is the Hamaker constant. As seen in equation 2.1, there is a direct proportionality between the magnitude of the van der Waals interaction energy and the Hamaker constant. The Hamaker constant is a materials constant that depends on the properties of the two materials and the intervening media. For both semi-infinite parallel

plates and two spheres,  $A_{123} < 0$  gives a positive  $F_{vdW}$  and repulsion occurs. The distance dependence of the van der Waals energy depends essentially on the geometry of the two interacting bodies, being proportional to  $L^{-2}$  for parallel plates and  $H^{-1}$  for two spherical particles at short separation distances where retardation can be ignored (less than 50 nm) [2-3].

## 2.2 Calculation of the Hamaker Constant

The major contribution to the Hamaker constant comes from frequencies in the visible and UV, and can be approximated using equation 2.5 [2-4].

$$A_{123} \equiv \frac{3}{4} kT \left( \frac{E_1 - E_2}{E_1 + E_2} \right) \left( \frac{E_3 - E_2}{E_3 + E_2} \right) + \frac{3}{8} \frac{h\nu_e}{\sqrt{2}} \frac{(n_1^2 - n_2^2)(n_3^2 - n_2^2)}{(n_1^2 + n_2^2)^{1/2} (n_3^2 + n_2^2)^{1/2} \{ (n_1^2 + n_2^2)^{1/2} + (n_3^2 + n_2^2)^{1/2} \}}$$

Eq. 2.5

The frequency  $\nu_e$  corresponds to the mean ionization frequency of the materials present. Typically this is  $\nu_e \approx 3 \times 10^{15}$  Hz.  $k$  is the Boltzmann's constant and  $h$  Planck's constant. The refractive indices for mediums 1, 2, and 3 are  $n_1$ ,  $n_2$ , and  $n_3$ , respectively.  $E_1$ ,  $E_2$ ,  $E_3$  are the static relative dielectric constants. The first term gives the zero-frequency energy of the van der Waals interaction and includes the Keesom and Debye dipolar contributions. For two non-polar media acting over a third medium, the first term is not significant compared to the second.

## 2.3 Self-Organized Batteries Using van der Waals Forces

In the proposed self-organized batteries, where repulsion is always desired between a cathode and anode for electronic isolation, while attraction between like particles of cathode and anode are desired for electronic connectivity, successful self-organization can be determined from the Hamaker constant ( $A_{123}$ ), where aggregation (+) or separation (-) of phases can be determined by the sign of the coefficient. The range of refractive

indices and dielectric constants determines the value of the Hamaker coefficient in a three-phase system. Having a system with a high dielectric constant ( $E$ ) or refractive index ( $n$ ) mismatch in a self-organized battery is beneficial in increasing the magnitude of  $A_{123}$ , and therefore helps in achieving a high repulsion between the two phases when  $n_1 > n_2 > n_3$ . As long as  $n_2 > n_3$ , the Hamaker constant will be negative. The larger the difference  $n_1 - n_2$ , the more negative is  $A_{123}$ . Of 31 polymer-solvent-polymer systems tested by C.J. Van Oss et al [2-5], 16 had a positive  $A_{123}$  and were therefore miscible. 11 had a negative  $A_{123}$ , and the two polymers were immiscible. However, four systems had very small values of  $A_{123}$ , between  $-0.9 \times 10^{-15}$  and  $+2.1 \times 10^{-15}$  erg and two of these four values gave rise to inaccurate predictions. Therefore, Van Oss concluded that accurate compatibility or incompatibility of a system can be predicted at Hamaker coefficient values of  $>3.0 \times 10^{-15}$  erg or more negative than  $-3.0 \times 10^{-15}$  erg, respectively [2-5]. Interestingly, in 1937, Hamaker generalized  $A_{123}$  for particles embedded in a fluid to vary between  $10^{-14}$  to  $10^{-11}$  erg as extreme limits and to lie between  $10^{-13}$  to  $10^{-12}$  erg in most cases [2-1].

In order to have a large selection of materials for self-organized batteries, either the cathode or anode must be of low refractive index. The refractive indices of organic solvents and binders range typically from 1.40 to 1.59. Thus, the closer the refractive index of either the cathode or anode to 1.40, the greater the selection of solvents and polymers available to satisfy  $n_1 < n_2 < n_3$ . However, if the lowest refractive index material, either cathode or anode, is 1.7, the number of organic solvents commercially available with  $n$  greater than 1.7 is less than 10. No documented polymer binders used for electrochemical cells have a refractive index greater than 1.7.

## 2.4 SBS Comparison with Conventional Cylindrical Cells: Performance Gains from the Interpenetrating Design

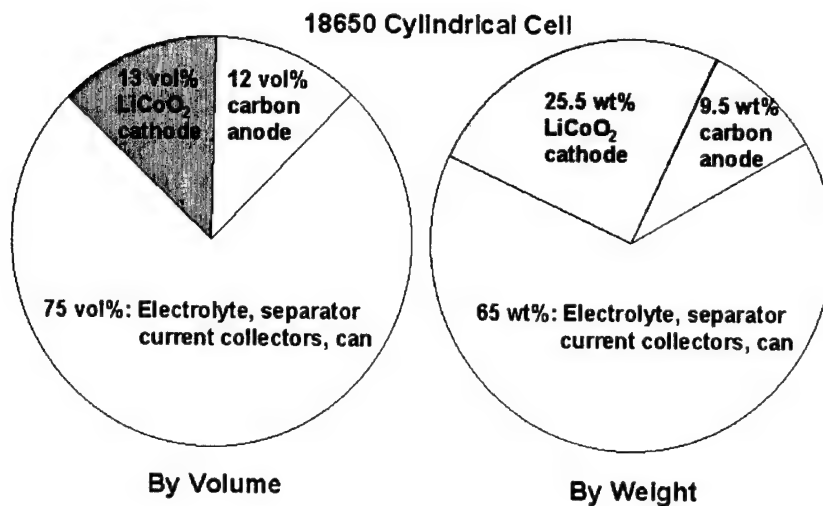


**Figure 2.2** Weight% and volume% analysis of conventional Li ion cells.

Conventional Li ion cells have poor volumetric and gravimetric utilization of the storage materials. For comparison, in a typical 18650 cylindrical cell (Figure 2.2), 75 vol% or 65 wt% is taken up by electrolyte, current collectors, and packaging materials. In the separator free, SBS design, greatly increased energy density could be achieved by reduction in the amount of electrolyte and separator required for electronic isolation of the anode and cathode. We estimate that 50 vol% solids packing could be easily achieved, resulting in about a factor of two increase in energy density.

Furthermore, the self-organized battery system allows for the nanoscale approach of the cathode and anode. Force/distance curves for repulsive van der Waals forces by Sigmund and Lee [2-6] show that repulsive interactions based on negative Hamaker constants between two dissimilar particles in an intervening medium begin to dominate at

distances from 6-10 nm. This allows for a shorter diffusion length of  $\text{Li}^+$  and should result in an increase in power density.

Models and experiments for conventional batteries have demonstrated that *the rate-limiting transport step is in most instances  $\text{Li}^+$  ion diffusion through the liquid-filled pore channels of the composite electrode* [2-7,2-8]. Thus, by reducing the Li ion diffusion distance to at best a few nanometers, or even to just a few microns, the power density gain over current technologies is expected to be one to two orders of magnitude.

However, other factors must be considered that could be rate limiting as well.

Particularly, the low electronic conductivity of conventional cathodes may have to be increased to take full advantage of the power density available in the interpenetrating design.

Furthermore, the quest by many researchers for the past 20 years to commercially implement a pure solid polymer electrolyte (SPE) may finally be realized with such an interpenetrating design. The best SPE's on the market today have room temperature conductivities of  $10^{-4}$  S/cm, which is still an order of magnitude below that of liquid electrolytes. By incorporating a SPE into the SBS design, additional packaging requirements that are required with liquid electrolyte cells could be removed, further reducing the weight of the electro-inactive materials and increasing the energy density of the cell.

## 2.5 References

- 2-1. H.C. Hamaker, "The London-van der Waals Attraction Between Spherical Particles", *Physica IV*, No. 10, 1058-72 (1937)
- 2-2. L. Bergstrom, "Hamaker Constants of Inorganic Materials", *Advances in Colloid and Interface Science*, **70**, 127 (1997)
- 2-3. R.J. Hunter, *Foundations of Colloid Science*, 2<sup>nd</sup> Ed, Clarendon Press, Oxford, 2001. J.N. Israelachvili, *Intermolecular and Surface Forces*, Academic Press, London, 1992.
- 2-5. C.J. Van Oss, D.R. Absolom, A.W. Newmann, "Applications of Net Repulsive Van Der Waals Forces Between Different Particles, Macromolecules, or Biological Cells in Liquids," *Colloids and Surfaces*, **1**, 45-56, (1980)
- 2-6. S. Lee and W. Sigmund, "Repulsive Van Der Waals Forces for Silica and Alumina", *Journal of Colloid and Interface Science*, **243**, 365-369 (2001)
- 2-7. M. Doyle, T.F. Fuller, J. Newman, *J. Electrochem. Soc.*, **140**, 1526-33 (1993)
- 2-8. B. Hellweg, "Microstructural Modeling of Lithium Battery Electrodes", S.M. Thesis, MIT, September 2000.

## **CHAPTER 3. Electronically Conductive Polymer Blends and Their Application to the SBS Concept**

### **3.1 Introduction**

The materials requirements for self-organized battery systems outlined in the previous chapter narrows the scope of usable cathode materials. To date, all secondary lithium cells have used approximately 10 wt% of a carbon additive in the cathode in order to ensure adequate electronic percolation. The SBS design is based on independent cathode and anode networks that are electronically conductive, and use only particle contacts to accomplish electronic percolation. A cathode material with potentially low enough refractive index and reasonable electronic conductivity is doped  $\text{LiFePO}_4$  olivine [3-1].  $\text{LiFeSO}_4$ , with a refractive index value of 1.54 [3-1], was explored briefly, but the compound was found to be too insulating in its undoped state. Conventional Li ion cathode materials such as  $\text{LiCoO}_2$ ,  $\text{LiMnO}_2$ , and  $\text{LiMn}_2\text{O}_4$  all have refractive index values of approximately 2.5, which would rule out the use of most organic separators/binders as the intervening material 2 [3-2]. However, one way to use conventional Li ion cathode materials in such an interpenetrating structure is to coat the cathode particles with an electronically and ionically conductive organic coating as displayed in Figure 3.1.



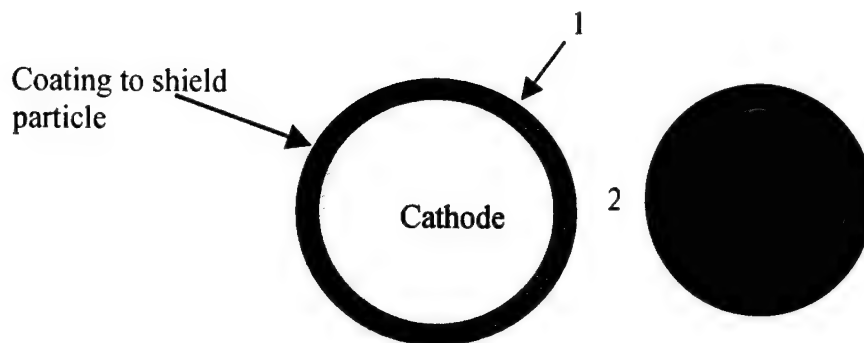


**Figure 3.1** Demonstration of low refractive index, electronically conductive polymer coating on the cathode in order to give  $A_{123} < 0$ .

One class of electronic/ionic conductive coatings can be conductive polymers and their blends. Another class may be sol-gel oxides. In this study, only conductive polymers were explored.

The first conductive polymer, polyacetylene, was discovered by accident in the 1970's by Heeger, MacDiarmid, and Shirakawa. They received the Nobel Prize for the discovery in 2000. Polyacetylene has a conductivity of 10,000 S/cm, but is highly unstable and decomposes quickly, even under inert atmosphere. Since then, numerous other conductive polymers of greater stability have been studied. A summary of some properties of the main groups of conducting polymers is listed in Table 3.1 [3-3].

Polymer	Conductivity (S/cm)	Stability (doped state)	Processing Possibilities
Polyacetylene	$10^3$ - $10^5$	Poor	Limited
Polyphenylene	1000	Poor	Limited
Poly( <i>p</i> -phenylene vinylene)	1000	Poor	Limited
Polypyrrole	100	Good	Good
Polythiophene	100	Good	Excellent
Polyaniline	10	Good	Good

**Table 3.1** Summary of conductive polymers available.

## **3.2 POMA/PVdF Conductive Blends**

### **3.2.1 Introduction**

All of the above mentioned conductive polymers are opaque, and little documentation exists regarding their refractive index values. Polyaniline (PANI) is one of the most studied due to its low cost and ease of processing. However, PANI has an average refractive index value of over 1.8 [3-4], which greatly reduces the available refractive index window for organic binders/electrolytes to be used as the intervening medium, when PANI is used as the coating. Thus, in order to lower the refractive index of the conductive coating, blends of an electronically conductive polymer with a low refractive index insulating polymer were considered in this work.

Poly(vinylidene fluoride) (PVdF) blends with PANI derivatives are well-studied with respect to their conductivity, processing, and miscibility [3-5]. Methoxy and ethoxy

substituted PANI show complete miscibility with PVdF when combined from dimethylformamide (DMF) co-solvent. Undoped PANI is soluble in DMF, but is immiscible with PVdF when DMF is the co-solvent. The alkyl substituents on PANI greatly increase its solubility, with a slight decrease in electrical conductivity compared to parent PANI.

Conductive polymers in their insulating (undoped) state are referred to as emeraldine base (EB). Upon addition of a conventional acid, such as hydrochloric acid (HCl), trifluoroacetic acid (TFA), or toluene sulfonic acid (TSA), the polymer becomes conductive. Electronic conduction occurs through generally a p-type mechanism along the  $sp^2$  conjugated backbone. A few n-type conductive polymers do exist [3-6]. The EB can be doped using three different doping methods: 1) doping the polymer in the powder form before dissolution, 2) first dissolving the undoped polymer and then doping it by adding concentrated acid to the solution, or 3) doping the polymer in the form of a film. Of the three doping methods, none appears to be superior to the others with respect to the electronic conductivity that is achievable.

The first system I examined for use in electronic isolation experiments was 10 wt% poly(*o*-methoxyaniline) (POMA) and 90 wt% poly(vinylidene fluoride) (PVdF). This combination allows for flexible, free-standing and stretchable films. Blends of conducting/insulating polymers can allow the best properties of both to be realized. This blend provides the electronic conductivity of POMA and the mechanical strength of PVdF. Conducting polymers cast by themselves are highly crystalline due to the rigid backbone of the  $sp^2$  hybridized system. Blending of POMA with PVdF at low wt% POMA allows for suitable electronic conductivity and films that can easily be cast (e.g.,

onto a glass substrate) and removed in one piece for analysis and further experimentation. The composition 10 wt% POMA/90 wt% PVdF was selected, for which the literature gives a room temperature conductivity value of  $5 \times 10^{-4}$  S/cm [3-5].

### **3.2.2 Synthesis of Conductive Polymer Blends**

Separate stock solutions of PVdF and TFA doped POMA were first prepared using N,N-dimethylformamide (DMF) as the co-solvent. A PVdF (534,000 M.W.) solution in DMF with a concentration of 0.0989 g/ml was prepared by mixing the appropriate amounts of starting materials and stirring at 70° C for approximately 20 minutes, where upon complete dissolution occurred.

A POMA stock solution with a concentration of 0.0171 g/ml was prepared. 9 vol% of TFA dopant relative to the TFA and the DMF was added. POMA EB was first dissolved in DMF at 70° C. Once the POMA was completely in solution, the TFA was added. Doping could be instantaneously observed by the color change from a bright blue to a dull green solution.

Appropriate amounts of the stock POMA and PVdF solutions to obtain 10 wt% POMA/ 90 wt% PVdF in the dried film were then combined and stirred vigorously for three minutes at room temperature. The solution, which was completely miscible, was then cast with a pipette onto a glass slide and dried under vacuum for 12 hrs. at room temperature. Conductive films approximately 15  $\mu$ m thick were obtained.

## **3.3 Conductivity Measurements of Polymer Blends**

### **3.3.1 Experimental**

A film of 10 wt% POMA/90 wt% PVdF (TFA doped) composition was cast onto a glass slide using the synthesis technique of section 3.2.2. The film dimensions were 5.0

mm, 0.030 mm, and 25 mm (Figure 3.2). Ag paint leads were attached to the ends of the film. A two-point conductivity measurement was taken in air immediately upon removal of the film from the vacuum oven.

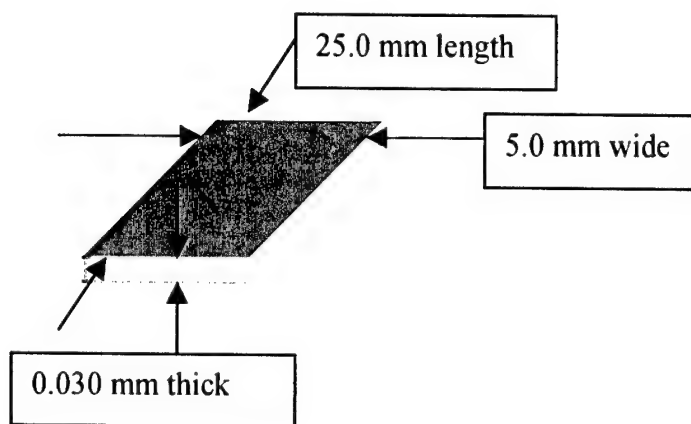


**Figure 3.2** 10 wt% POMA/90 wt% PVdF dimensions with Ag paint leads on the ends for electronic conductivity measurements. The film was cast onto a glass substrate.

### 3.3.2 Observations

A two-point resistance of  $14 \text{ M}\Omega$  was observed across the  $1.5 \times 10^{-3} \text{ cm}^2$  area by 2.5 cm length sample. This corresponds to a resistivity of  $8400 \text{ }\Omega\text{cm}$ , and a conductivity of  $1.19 \times 10^{-4} \text{ S/cm}$ .

### 3.3.3 Conclusions

The measured conductivity value of  $1.19 \times 10^{-4} \text{ S/cm}$  is in good agreement with the literature value of  $5 \times 10^{-5} \text{ S/cm}$  for the same composition of 10 wt% POMA/90 wt% PVdF and using TFA as a dopant [3-5]. This conductivity value is assumed sufficient for

electronic conductivity in a cathode network if it can successfully be coated onto a cathode particle.

### **3.4 Refractive Index Measurement of 10 wt% POMA/90 wt% PVdF Conductive Blend**

The 10 wt% POMA/90 wt% PVdF (TFA doped) composition was selected since it provides sufficient conductivity as well as potentially a low refractive index. PVdF has a refractive index of 1.42. The goal was to achieve adequate electronic conductivity while keeping the refractive index as low as possible.

#### **3.4.1 Experimental**

Ellipsometry measurements were taken of the opaque films cast on glass slides using the Gaertner Single Wave Ellipsometer Model L3W26C operating at 633 nm.

#### **3.4.2 Observations**

A refractive index value of 1.46 was obtained for the 10 wt% POMA/90 wt% PVdF (TFA doped) polymer blend. Figures 3.3 (a) and (b) show SEM images of the dried films of 10 wt% POMA/90 wt% PVdF (TFA doped) polymer blend. The morphology observed is similar to that of pure PVdF, which also dries in 4-6  $\mu\text{m}$  diameter spherical particles. The electronically connected POMA network is dispersed within the spherical particles and at the particle necks.

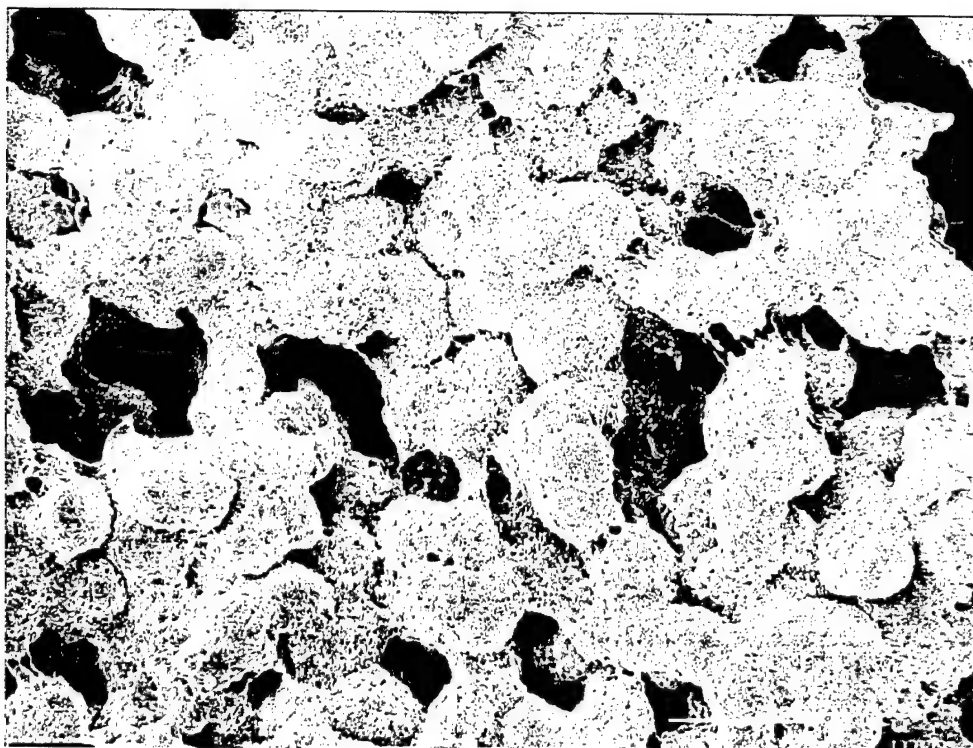


**Figure 3.3 a** SEM analysis of 10 wt% POMA/90 wt% PVdF (TFA doped)

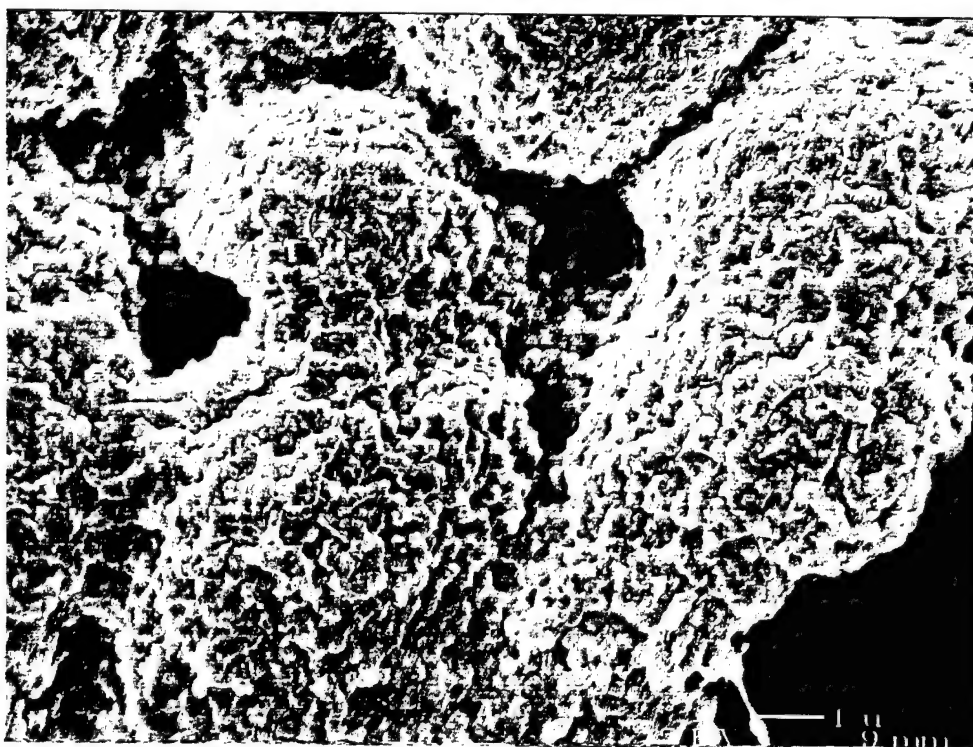


**Figure 3.3 b** SEM analysis of 10 wt% POMA/90 wt% PVdF (TFA doped)

### **3.4.3 Conclusions**

An electronically conductive, low refractive index POMA/PVdF blend was identified and prepared. The measured refractive index value of 1.46 allows multiple options for organic electrolyte/binders as the intervening material 2 in a self-organized battery, since these materials have refractive indices that typically range from 1.45-1.59.

### **3.5 Coating of Particles with a 10 wt% POMA/90 wt% PVdF Conductive Blend**

Limited attempts were made at open-air milling of  $\text{LiCoO}_2$  and MCMB with the conductive blend solution in DMF, using Teflon balls. Upon drying; however, uniform coatings did not result at the particle scale. Instead, the batch of powder and polymer was severely agglomerated. Due to time limitations, particle-coating processes were not investigated in greater detail.

### **3.6 Summary**

A conductive polymer blend was established that can serve as a low refractive index end member of a self-organized battery. This application of particle coatings deserves further attention as a method for obtaining low refractive index, electronically, and ionically conductive materials. It may allow a solid polymer electrolyte (SPE) such as PEO to be used in an SBS cell. High molecular weight PEO has a refractive index range of 1.51-1.54; therefore, a negative Hamaker would be maintained when PEO is the intervening medium between the conductive blend and the high refractive index anode. Depending upon the polymer chain mobility in the solid state, it could also be a dynamic, self-repairing system.



### 3.7 References

- 3-1. <http://www.hbcnetbase.com/hbcnet/Toc.jsp?SpaceID=10093&BookID=34&NodeID=109243040#node109243040> CRC Online Handbook, Physical Constants of Inorganic Compounds.
- 3-2. <http://www.hbcnetbase.com/hbcnet/Toc.jsp?SpaceID=10093&BookID=34&NodeID=109243037#node109243037> CRC Online Handbook, Physical Constants of Organic Compounds.
- 3-3. M. Rubner, Course 3.98-Polymer Synthetic Chemistry, MIT, Fall Semester (Academic yr 2000-01)
- 3-4. <http://www.ntcresearch.org/pdf-rpts/Bref0596/G95-08.pdf> National Textile Center Research Briefs: May 1996
- 3-5. L.F. Malmonge, L. Mattoso, *Polymer*, **36**, No. 2, 245-249, (1995)
- 3-6. S. Janietz, S. Anlauf, A. Wedel, *Synthetic Metals*, **122**, 11-14, (2001)

## CHAPTER 4. Electronic Isolation Experiments

In order to have a self-organized battery system, a bipolar electrochemical junction has to be established. Having a system with a high dielectric constant ( $\epsilon$ ) or refractive index ( $n$ ) mismatch in a self-organized battery is beneficial in increasing the magnitude of  $A_{123}$ , and therefore helps in achieving a high repulsion between the anode and cathode phases when  $n_1 > n_2 > n_3$ . As long as  $n_2 > n_3$ , the Hamaker constant will be negative. The larger the difference  $n_1 - n_2$ , the more negative is  $A_{123}$ .

Four experiments were conducted to test for electronic isolation in a layered geometry between two conductive materials between which  $A_{123} < 0$  is expected. In layered experiment 1, a polymer blend of 10wt% poly(*o*-methoxyaniline) (POMA)/90wt% poly(vinylidene fluoride) (PVdF) was cast and dried as a free standing film, and layered on top of a wet casting of a MCMB/PEO/diiodomethane (DIM) layer. The expectation was that the low refractive index conductive polymer film would be isolated from the high refractive index MCMB due to a repulsive dispersion force.

In layered experiment 2,  $\text{LiMg}_{0.05}\text{Co}_{0.95}\text{O}_2$  (LMCO) powder in a PEO/DIM solution was cast onto a POMA/poly(acrylonitrile) (PAN) conductive film, with the expectation that the LMCO would be isolated from the conductive film.

In layered experiment 3, LMCO in a PS/DIM solution was cast onto a 10 wt% POMA/90 wt% PVdF film, again with the expectation that the LMCO would be isolated from the conductive film.

In layered experiment 4, MCMB in a PS/1,2-diiodoethane (DIE) solution was cast onto a solid film containing 80 vol% LFP/20 vol% PVdF (534K MW). The DIE medium was expected to electronically isolate the MCMB from the LFP. In all four systems, a

low refractive index ( $n_1$ ) and a high refractive index ( $n_3$ ) electronically conductive material is used with an intervening fluid of intermediate refractive index ( $n_2$ ).

Therefore,  $n_1 < n_2 < n_3$ , and  $A_{123} < 0$  is expected.

#### **4.1 Layered POMA/PVdF-PEO/DIM-MCMB Isolation Experiment**

##### **4.1.1 Experimental**

A suspension consisting of MCMB dispersed in a solution of DIM and PEO was tape cast using a 254  $\mu\text{m}$  thick stencil onto a glass slide. Three different MCMB/PEO ratios were prepared: 40 vol% MCMB/60 vol% PEO, 50 vol% MCMB/50 vol% PEO, and 60 vol% MCMB/40 vol% PEO. PEO of 200,000 M.W. was used. In all three cases, 1 g of MCMB was used and the appropriate amount of PEO was added. It was observed that uniform casting resulted when the PEO was 10 vol% of the total volume of polymer and solvent. While still wet, the casting was immediately covered with a strip of the conductive polymer blend 10 wt% POMA/90 wt% PVdF (Figure 4.1), prepared according to the experimental description in Chapter 3. Electronic isolation between the low refractive conductive polymer blend and the high refractive index MCMB is expected to be observed with DIM as the intervening medium. The samples were then dried under vacuum at room temperature for 12 hrs. The films of POMA/PVdF blend varied from 15-30  $\mu\text{m}$  in thickness and the MCMB/PEO layer was approximately 100  $\mu\text{m}$  thick when dry.

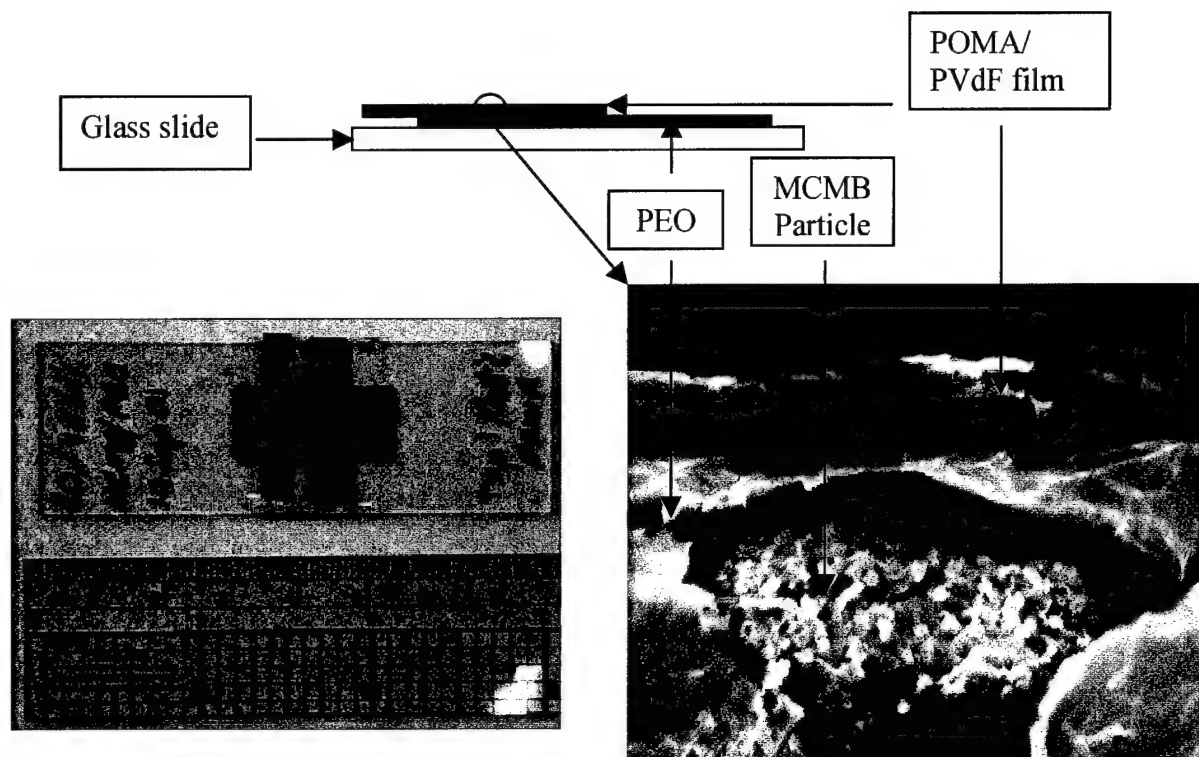


**Figure 4.1** Experiment demonstrating electronically insulating junctions between two conductive materials in a system expected to have a negative Hamaker constant. Cross-section SEM analysis shows the PEO wetting between the MCMB and the conductive polymer blend as expected for  $A_{123} < 0$ , where 1 is the conductive polymer blend, 2 is the DIM, and 3 is the MCMB.

#### 4.1.2 Observations

The refractive index of 10wt% POMA/90wt% PVdF (TFA doped) was previously measured by ellipsometry at 633 nm wavelength illumination and determined to be 1.46 ( $n_1$ ). The refractive index of MCMB is 2.5 ( $n_3$ ) and that of diiodomethane is 1.7411 ( $n_2$ ). Thus,  $n_1 < n_2 < n_3$ , and  $A_{123} < 0$  is expected (Figure 4.1).

Figure 4.2 shows where resistance measurements were taken once the diiodomethane was removed from the system by vacuum drying at room temperature for 12 hrs. Table 4.1 shows the resistance value and the separation distance between the two probes for an experiment where 60 vol% MCMB/40 vol% PEO was used.

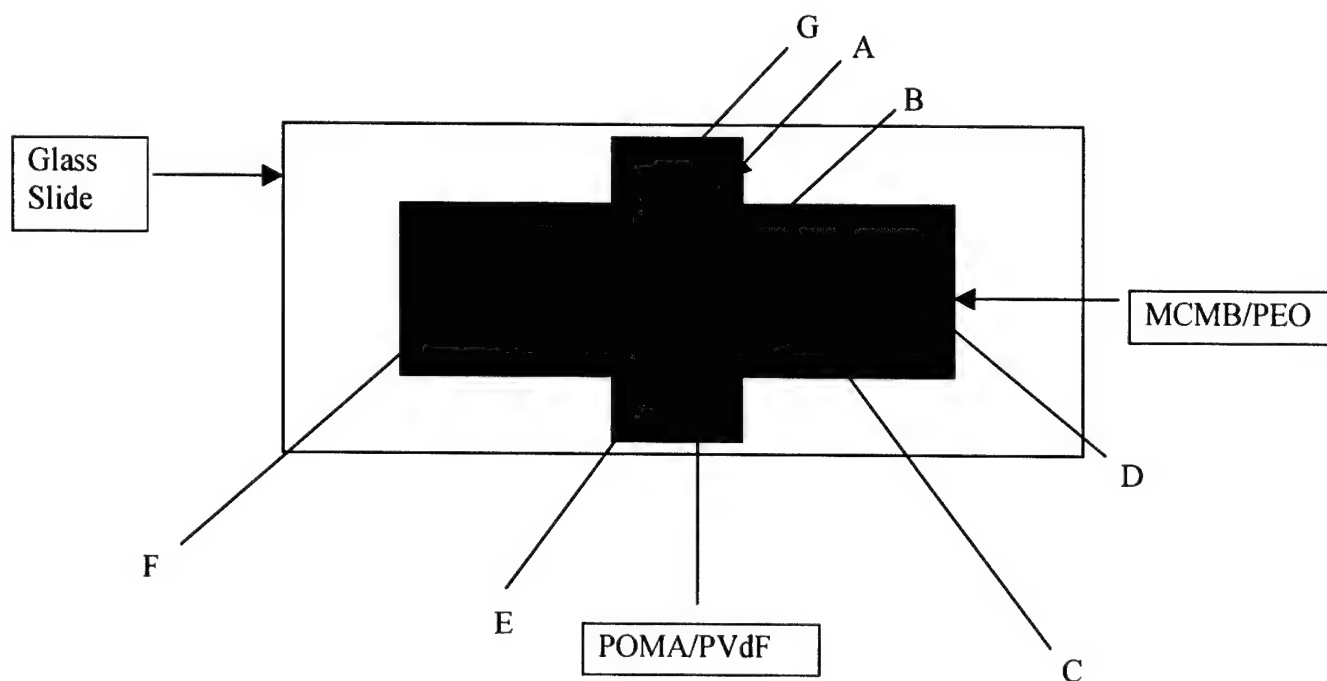


**Figure 4.2** Experimental configuration for measuring resistance across each conductive film and between the two films.

	A	B	C	D	E	F	G
A		1.2 M $\Omega$ 3-4 mm			1.0 M $\Omega$ 1.5 cm		0.5 M $\Omega$ 3-4 mm
B	1.2 M $\Omega$ 3-4 mm		60k $\Omega$ 3-4 mm				
C		60k $\Omega$ 3-4 mm					
D						360 k $\Omega$ 2 cm	
E	1.0 M $\Omega$ 1.5 cm						
F				360 k $\Omega$ 2 cm			
G	0.5 M $\Omega$ 3-4 mm						

**Table 4.1** Resistance measurements recorded between films of POMA/PVdF and 60 vol% MCMB/40 vol% PEO. The separation distance between the two probes corresponds to the measurement points referenced in Figure 4.2. Points A, G, and E correspond to the POMA/PVdF film and points B, C, D, and F correspond to the MCMB/PEO film.

The resistance across 3-4 mm of the MCMB/PEO film was 60k $\Omega$ . The resistance across 3-4 mm of POMA/PVdF film was 0.5 M $\Omega$ . Interestingly, between the POMA/PVdF and the MCMB/PEO films, the 2-point resistance between points A and B (3-4 cm) was 1.2 M $\Omega$ . Amongst the samples prepared, this was the lowest value recorded across the two films. Approximately 2 M $\Omega$  was observed when a 40 vol% MCMB/60 vol% PEO film was utilized. Thus, the through layer resistance between the two conductive layers shows an additional interfacial resistance from 0.7 M $\Omega$  to 1.5 M $\Omega$  that would not be present if the two layers were electronically shorted. This experiment

was repeated with the three different volume fractions of MCMB/PEO and 5 samples of each composition. An additional interface resistance was observed in each instance.

#### **4.1.3 Conclusions**

This experiment clearly demonstrates the existence of an additional interface resistance. Electronic isolation between the two layers is clearly occurring, consistent with the result expected for  $A_{123} < 0$ . However, other factors could also contribute to the observed additional interfacial resistance. First, the DIM in the PEO/MCMB castings could have dedoped the POMA/PVdF. As well, the PEO could wet between the POMA/PVdF and the MCMB for reasons other than having  $A_{123} < 0$ . Finally, the resistance of the POMA/PVdF films may differ between the through-thickness and in-plane directions.

### **4.2 Layered Ag-POMA/PAN-PEO/DIM-LMCO Experiment**

#### **4.2.1 Motivation for a POMA/PAN Polymer Blend**

A POMA/PAN blend is an attractive composition since POMA is a good electronic conductor and PAN is a reasonably good SPE when doped with  $\text{LiClO}_4$ , with a conductivity value of  $5 \times 10^{-6} \text{ S/cm}$  at room temperature [4-1]. Thus, if this blend could be coated onto the surface of either cathode or anode, then the requirements of a low refractive index and electronic and ionic conduction could potentially be met.

#### **4.2.2 Experimental**

The POMA solution was prepared according to the specifications outlined in Chapter 3. PAN was substituted for PVdF and co-solubility of POMA and PAN in DMF was observed. The PAN stock solution concentration was 0.0989 g/ml. The PAN solution was doped with  $\text{LiClO}_4$  at 20 wt% of polymer and salt (1:4, Li:CN) in order to achieve

ionic conductivity. The POMA and PAN/LiClO<sub>4</sub> stock solutions were then combined to give a dry film with 10 wt% POMA/90 wt% PAN. The films were dried under vacuum at room temperature for 12 hrs. and immediately transferred to the Argon filled glovebox. All samples were handled in the glovebox once dry due to the hygroscopic nature of the salt-doped polymer blend. The films were applied to silver foil substrates, which also serve as a metal anode, since Ag can be lithiated up to a concentration of LiAg.

A suspension of LiMg<sub>0.05</sub>Co<sub>0.95</sub>O<sub>2</sub> (LMCO) powder in a solution of PEO and DIM with the PEO being 10 vol% of the total volume of polymer and solvent was heated to 50° C with continuous stirring. Once the PEO was dissolved, the LMCO/PEO/DIM slurry was cast onto the POMA/PAN substrates (Figure 4.3). Once the LMCO/PEO was cast, the entire sandwich was dried under vacuum at room temperature for 12 hrs. Additionally, separate samples of LMCO/PEO/DIM slurry were cast onto a glass slide and dried at room temperature for 12 hrs. under vacuum for electronic conductivity measurements.

#### **4.2.3 Observations**

When the electrodes of the multimeter were placed 3-4 mm apart on the PEO/LMCO film cast onto glass, resistances of 1-2 MΩ were observed for a film thickness of 100 μm. The 2-point resistance measured through the POMA/PAN to the Ag foil was approximately 1 MΩ. However, after the LMCO/PEO layer was cast onto the Ag foil coated with the POMA/PAN conductive blend, and dried, the two-point resistance measured through all three layers is greater than 5 MΩ. This sample was placed in a stainless steel screw-top electrochemical cell and flooded with LP 30 (1:1 EC:DMC, 1 M LiPF<sub>6</sub>) liquid electrolyte. An open circuit voltage of 0.72 V was observed. However, due



to the solubility of PEO in liquid electrolyte, the cell shorted after approximately 30 minutes. This prevented further electrochemical testing.

Stereomicroscope inspection of the POMA/PAN layer showed that phase separation was occurring, probably into a POMA-rich and PAN-rich phase. No literature data was found for this conductive blend. The effect of the phase separation on the electronic isolation behavior is presently unknown.

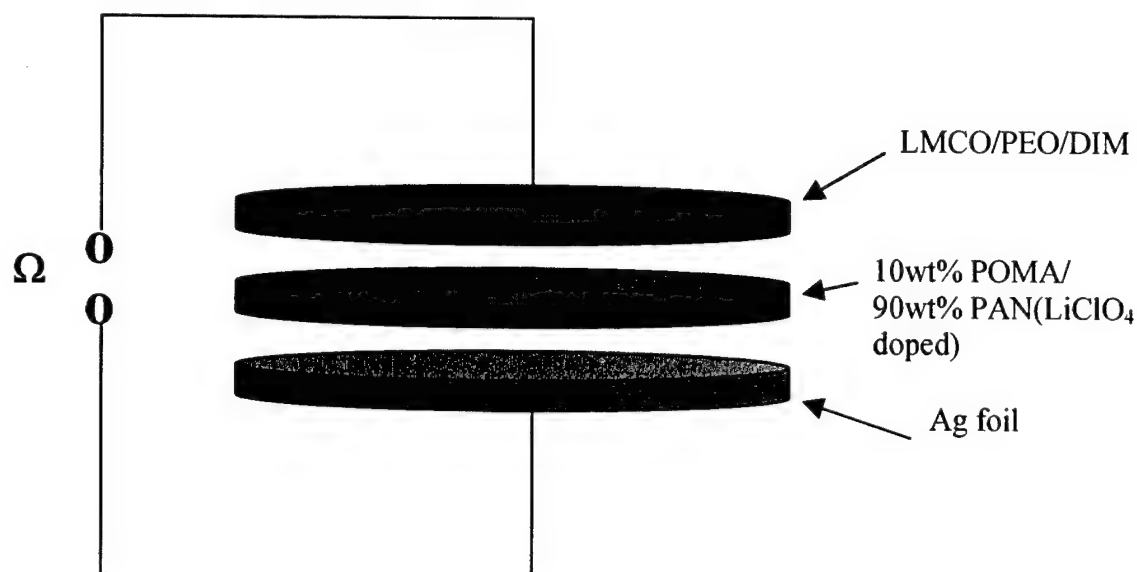


**Figure 4.3** Schematic of the through layer resistance measurement showing electronic isolation between LMCO and POMA/PAN.

#### 4.2.4 Conclusions

A negative  $A_{123}$  is expected to exist between the LMCO and the POMA/PAN when it is separated by the PEO/DIM solution. Here also, electronic isolation between the percolating conductive network of LMCO and the conductive polymer film appears to have been achieved, resulting in an additional interfacial resistance of approximately 4 M $\Omega$ .

### 4.3 Layered LMCO-PS/DIM-POMA/PVdF Isolation Experiment

#### 4.3.1 Experimental

The POMA/PVdF blend was cast and dried on Ag foil discs 3/8ths inch diameter and 100  $\mu\text{m}$  thick according to the experimental section of Chapter 3. On top of the conductive polymer coating, a suspension of  $\text{LiMg}_{0.05}\text{Co}_{0.95}\text{O}_2$  (LMCO) powder and PS in DIM was cast (Figure 4.4). The ratio of LMCO to PS was 50:50 by volume. The PS (50,000 M.W.) was 10 vol% of the total volume of PS and DIM, and was dissolved by heating to 70° C with continuous stirring. Once the LMCO/PS suspension was cast, the entire sandwich was dried under vacuum at room temperature for 12 hrs. PS was used because it is soluble in DIM and insoluble in common liquid electrolytes. The samples were placed in a stainless steel screw-top electrochemical cell and wet with LP 30 (1:1 EC:DMC, 1 M  $\text{LiPF}_6$ ) liquid electrolyte and electrically connected for cycle testing.

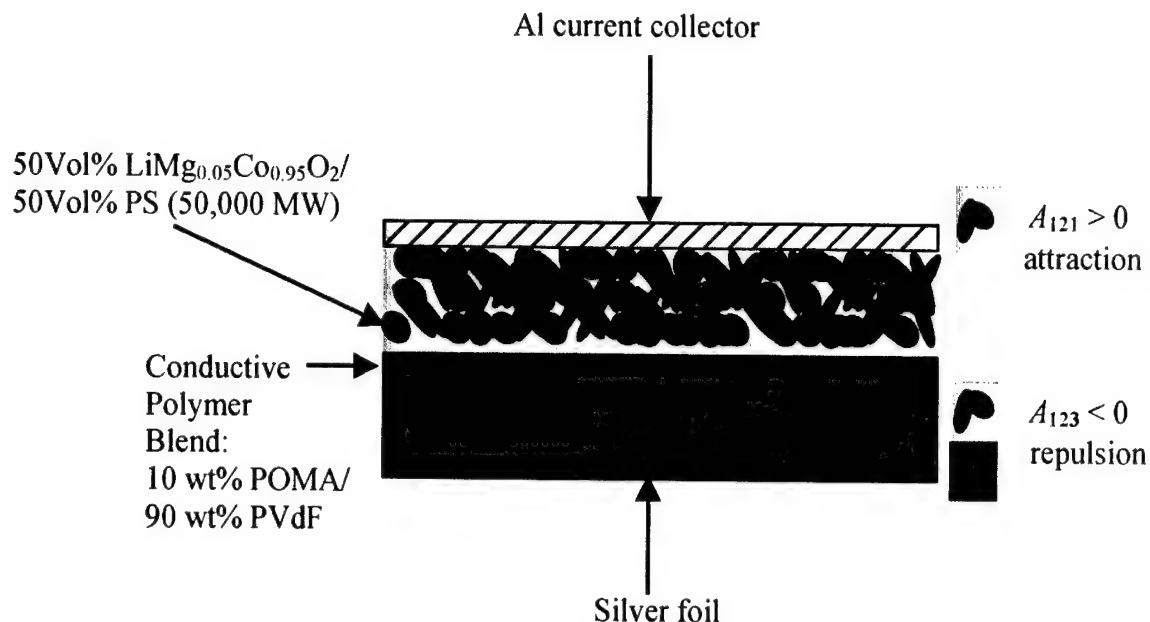


**Figure 4.4** Schematic of layered assembly for cycle testing.

#### 4.3.2 Observations

Figure 4.5 shows the voltage vs. capacity curve measured at a charging rate of 10mA/g. The upper voltage cut-off limit was set to 4 Volts. Once 4 V was reached, the system switched to discharge and the cell voltage fell to 0.7 V in approximately 60 seconds. 8 such cells were assembled, of which 5 were apparently shorted upon assembly since they showed no measurable voltage; however, 3 cells had an OCV of approximately 100 mV upon assembly and showed charging like behavior. The thermodynamic voltage for the removal of  $\text{Li}^+$  from LMCO and insertion into Ag metal is approximately 3.3 volts. The plateau from the charge curve in Figure 4.5 starts at 2.7 volts and extends up to 3.6 volts.

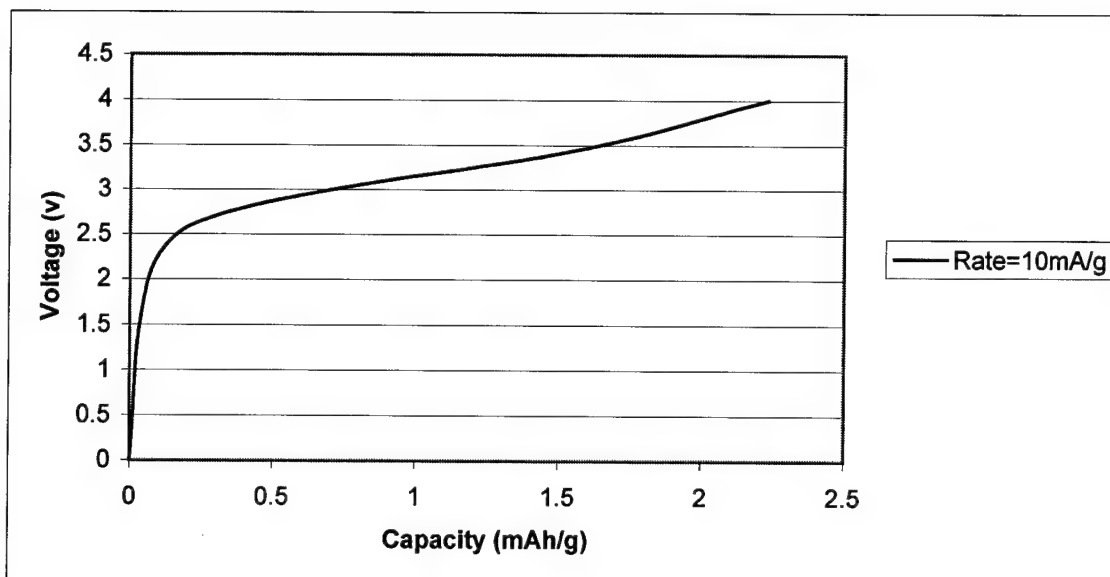


**Figure 4.5** Voltage vs. capacity for layered cell Ag-POMA/PVdF-PS/DIM-LMCO. The current rate and the capacity is calculated for the LMCO mass.

#### 4.3.3 Conclusions

Although the cells failed to show a significant discharge capacity, the plateau voltage observed is consistent with that expected for the LMCO/Ag couple, and the shape of the curve suggests that charging of the cell occurred. Although POMA is known to be electrochemically active [4-2], in the configuration in Figure 4.4, POMA is at the negative electrode and cannot contribute to the capacity observed.

#### 4.4 Isolation Experiments Using $\text{LiFePO}_4$

$\text{LiFePO}_4$  (LFP) is attractive as a cathode material for dispersion force self-organized batteries due to its low refractive index. It exists naturally as the mineral triphylite with the formula  $\text{Li}(\text{Fe},\text{Mn})\text{PO}_4$ , and has a reported refractive index of 1.69 [4-3]. Thus, the refractive index of DIM, with  $n=1.7411$ , is between the refractive index of  $\text{Li}(\text{Fe},\text{Mn})\text{PO}_4$  and MCMB and should allow electronic isolation between the two. However,  $\text{LiFePO}_4$  is insulating and requires a dopant in order to be electronically conductive. Group members

Dr. Sung-Yoon Chung and Jason Bloking have explored various dopants, including Ti, Nb, Zr, and Mg, that increase the conductivity of  $\text{LiFePO}_4$  by several orders of magnitude. The undoped powder is gray, whereas the doped powder is black. Dopants on both the Li site and the Fe site were explored. A 1% Nb doped sample of  $\text{LiFePO}_4$  that was pressed as a pellet and fired at  $850^\circ\text{C}$  had a measured refractive index of 1.78 at 633 nm wavelength illumination. However, this sample also had  $\text{Fe}_3\text{P}$  present as a second phase, which should raise the average index. This is above the refractive index of diiodomethane,  $n=1.7411$ , and thus would give  $A_{123}>0$  between MCMB and  $\text{LiFePO}_4$ .

#### 4.4.1 Experimental

A solid film containing 80 vol%  $\text{LiAl}_{0.01}\text{Fe}_{0.99}\text{PO}_4$  and 20 vol% PVdF (534K MW) was first tape cast using DMF as the solvent onto Al foil and dried in air at  $50^\circ\text{C}$ , to give 50  $\mu\text{m}$  thick films. Disks were subsequently cut out using a 3/8ths inch punch. A suspension of 60 vol% MCMB and 40 vol% PS (50K MW) was prepared with the PS 10 vol% of the total volume of PS and DIM. The PS dissolved at  $70^\circ\text{C}$  under constant stirring. The MCMB/PS/DIM suspension was cast onto the LFP/PVdF substrate with a pipette and the entire sandwich was dried at  $50^\circ\text{C}$  in air (Figure 4.6).

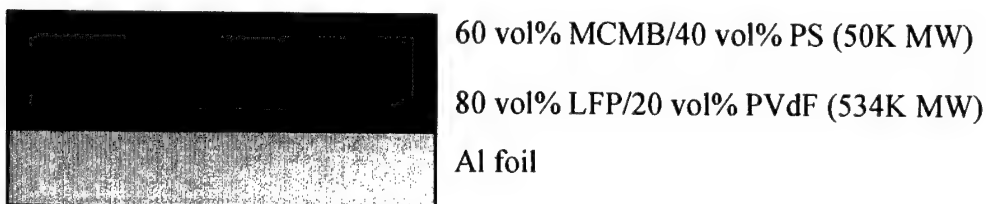


**Figure 4.6** Layered configuration where it is expected that the condition  $A_{123}>0$  will exist between the MCMB and the LFP.

#### 4.4.2 Observations

First, the conductivity of the LFP/PVdF layer was measured. Independent 4-point resistivity measurements performed by Jason Bloking of a sintered  $\text{LiAl}_{0.01}\text{Fe}_{0.99}\text{PO}_4$  pellet gives a value of  $\rho = 1 \times 10^3 \Omega \cdot \text{cm}$ . The through-layer resistance with a  $1 \text{ cm}^2$  Au electrode sputtered on top of the  $\text{LiAl}_{0.01}\text{Fe}_{0.99}\text{PO}_4/\text{PVdF}$  layer that was  $50 \mu\text{m}$  thick was  $3\text{-}5 \Omega$ . This is consistent with the resistivity measurement performed on the sintered pellet. A 2-point resistance measurement across  $1 \text{ cm}$  of the  $60 \text{ vol}\% \text{ MCMB}/40 \text{ vol}\% \text{ PS (50K MW)}$  film gives  $1\text{-}5 \text{ k}\Omega$ . When  $100\% \text{ DIM}$  was used as the solvent and intervening medium in  $A_{123}$ , the through-layer resistance from MCMB/PS casting to Al foil was  $1\text{-}5 \text{ k}\Omega$ . Although the through-layer resistance of the  $60 \text{ vol}\% \text{ MCMB}/40 \text{ vol}\% \text{ PS (50K MW)}$  layer should be significantly less than  $1\text{-}5 \text{ k}\Omega$  at a layer thickness of approximately  $100 \mu\text{m}$ , the low resistance of the sandwich indicates that the MCMB may have shorted to the  $\text{LiAl}_{0.01}\text{Fe}_{0.99}\text{PO}_4/\text{PVdF}$  casting. This apparent shorting is consistent with the measured refractive index value of doped LFP, giving  $A_{123} > 0$  when DIM is used as the intervening medium between MCMB and  $\text{LiAl}_{0.01}\text{Fe}_{0.99}\text{PO}_4$ .

#### 4.4.3 Conclusions

Electronic shorting between  $\text{LiAl}_{0.01}\text{Fe}_{0.99}\text{PO}_4$  and MCMB was observed when DIM was the liquid medium. From this result, it is concluded that the refractive index of the particular  $\text{LiAl}_{0.01}\text{Fe}_{0.99}\text{PO}_4$  used is probably above that of DIM ( $n=1.7411$ ). However, not all the doped LFP's are the same due to the possible presence of second phase ( $\text{Fe}_3\text{P}$ ) and excess carbon.

## **4.5 Isolation Experiments Substituting 1,2-diiodoethane (DIE) for diiodomethane (DIM)**

### **4.5.1 Experimental**

In order to observe electronic isolation between the doped LFP and MCMB, a higher refractive index solvent was believed to be necessary. 1,2-diiodoethane (DIE) is an attractive alternative to DIM as it has a listed refractive index of 1.871 [4-4].

DIE has a melting point of 83° C and is therefore solid at room temperature. PS is soluble in DIE at 100° C. A solids mixture containing 60 vol% MCMB/40 vol% PS (50K MW) was mixed with DIE. The DIE was 10 vol% of the total volume of polymer and solvent. The 3-component system was mixed in a sealed glass jar and placed in an oven at 100° C. The PS was mixed every 5 minutes, and after 15 minutes, appeared to have completely dissolved. Upon removal from the oven, pouring onto Al foil at room temperature quenched the 3-component system, whereupon solidification quickly occurred. The sample was then ground to break up large pieces. This MCMB/PS/DIE mixture was then cast onto substrates consisting of films of 80 vol%  $\text{LiAl}_{0.01}\text{Fe}_{0.99}\text{PO}_4$ /20 vol% PVdF (534K MW) prepared on Al foil. These substrates were prepared according to the procedure in 4.4.1. The  $\text{LiAl}_{0.01}\text{Fe}_{0.99}\text{PO}_4$  used here was from the same batch as that used in section 4.4. The MCMB/PS/DIE solid mixture was placed on top of the LFP/PVdF coated Al substrates that were punched out to 3/8ths inch diameter. The samples were then placed into the oven again at 100° C whereupon the DIE melted and evaporated from the sample. A Cu current collector was attached to the anode (MCMB) side after the sample was cooled (Figure 4.7).

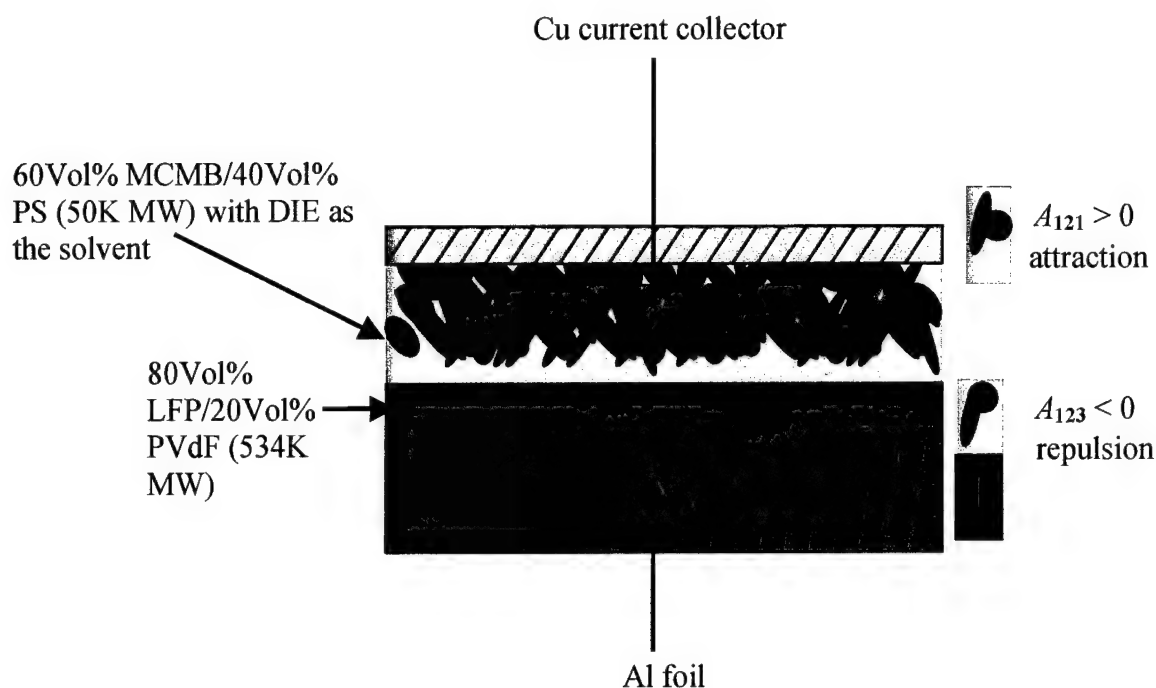


**Figure 4.7** Schematic of sample for electrochemical testing.

#### 4.5.2 Observations

Two point measurements of the through-layer resistance gave values of over 30 M $\Omega$  when DIE was used as the solvent. Across the MCMB/PS casting alone, the 2-point resistance measurement gave values from 1-5 k $\Omega$  when the probes were 3-4 mm apart. When a solution of only PS and DIE are dried at 100 $^{\circ}$ C, a clear, colorless, and uniform layer of PS is left behind, indicating that all of the DIE can be removed.

#### 4.5.3 Conclusions

The results show that when 1,2-diiodoethane (DIE) is used as the solvent for PS, and as the intervening medium between MCMB and LiAl<sub>0.01</sub>Fe<sub>0.99</sub>PO<sub>4</sub>/PVdF layer, electrical isolation clearly occurs between the two.



#### 4.6 Cell Preparation and Cycling Experiments

The samples described in section 4.5 were assembled into cells as shown in Figure 4.8 and then flooded with liquid electrolyte (LP 30).

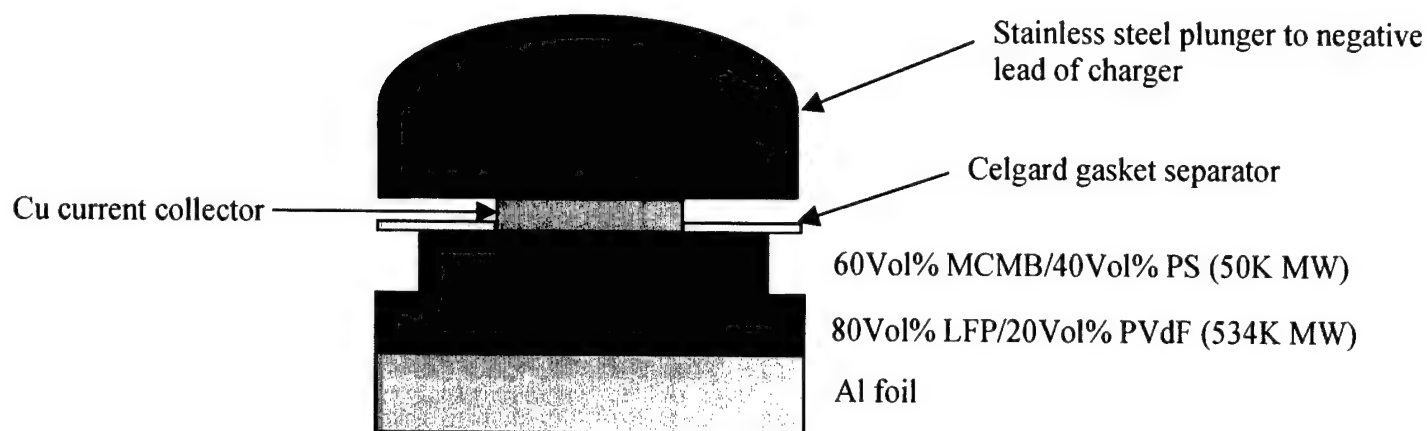


**Figure 4.8** Sample preparation for electrochemical testing.

The MCMB/PS coating did not cover the entire surface of the LFP/PVdF layer. Thus, a Celgard gasket was put in place to prevent the stainless steel plunger from shorting to the LFP/PVdF layer. Figure 4.9 is a charge curve for a cell cycled at room temperature.

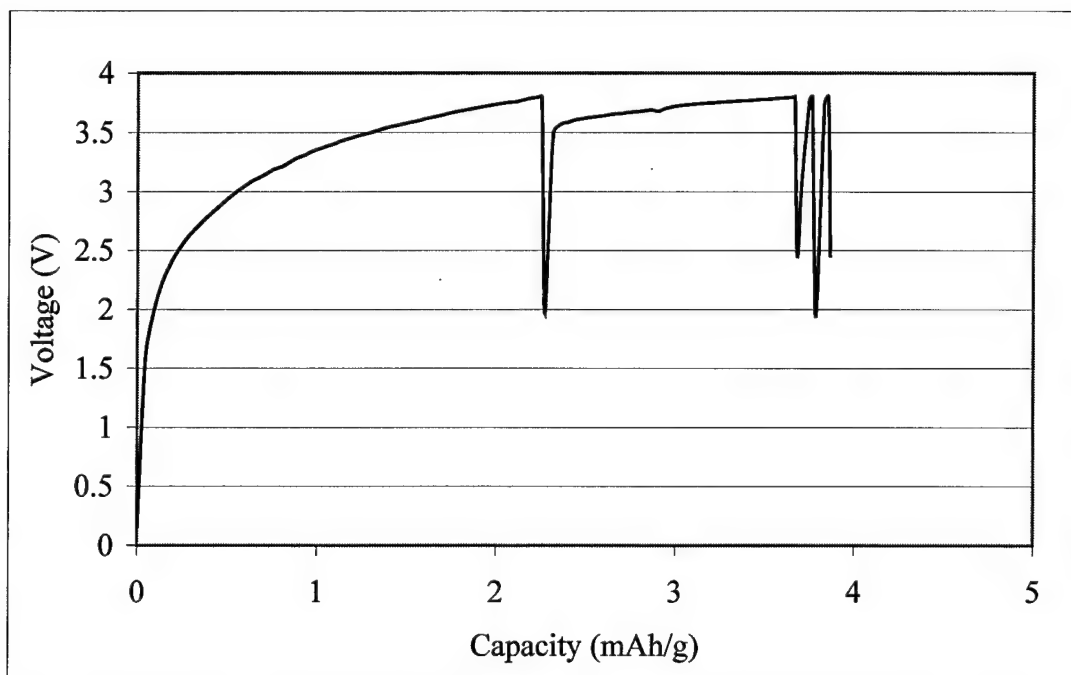


**Figure 4.9** Charge curve for cell of the configuration illustrated in Figure 4.8, tested at 25°C. The current rate and the capacity is calculated for LFP mass.

The voltage limits in Figure 4.9 were set at 2.5 V – 3.8 V and the charging current at a rate of 5 mA/g. When the voltage reached 3.8 V, the cell switched to discharge and the voltage immediately fell below the 2.5 V lower voltage limit. When the lower voltage limit was set to 0.005 V and the same cell was heated to 50°C, the charge/discharge curve in Figure 4.10 was obtained.

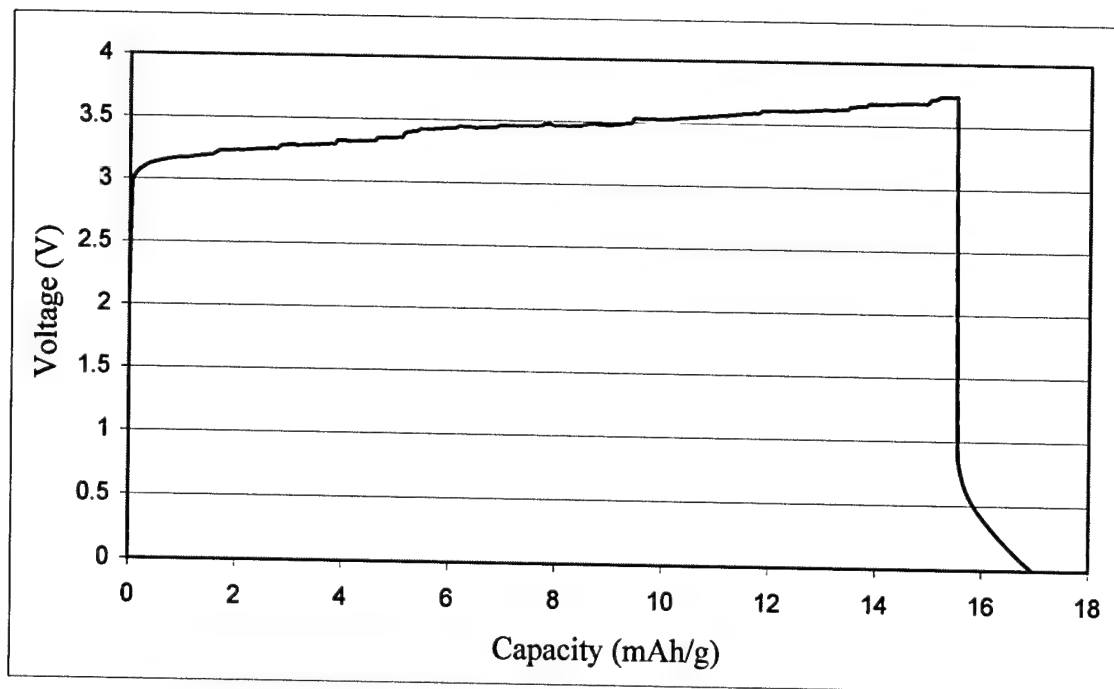


**Figure 4.10** Charge curve for cell of the configuration illustrated in Figure 4.8, tested at 50°C. The current rate and the capacity is calculated for LFP mass.

Thermodynamically, Li intercalation into LFP should occur at 3.25 V vs. MCMB. This is close to the charging voltage observed. Assuming that the voltage plateaus in Figures 4.9 and 4.10 are close to the equilibrium voltage, a much greater polarization is observed when the cell is discharged. In Figure 4.10, it appears that discharge begins at approximately 0.75 V. For comparison, undoped  $\text{LiFePO}_4$  was pressed as a pellet with 10 wt% PVdF as a binder and no carbon additive and cycled against Li using a Celgard separator in a conventional cell design (Figure 4.11) [4-5]. The thermodynamic intercalation voltage of  $\text{LiFePO}_4$  vs. Li is 3.5 V. In Figure 4.11, low polarization (100-200mV) is observed upon charging; however, as in the case of Figure 4.10, no discharge is observed. Thus, the same charge with failure to discharge behavior is observed in a cell with known electronic isolation provided by the Celgard separator.

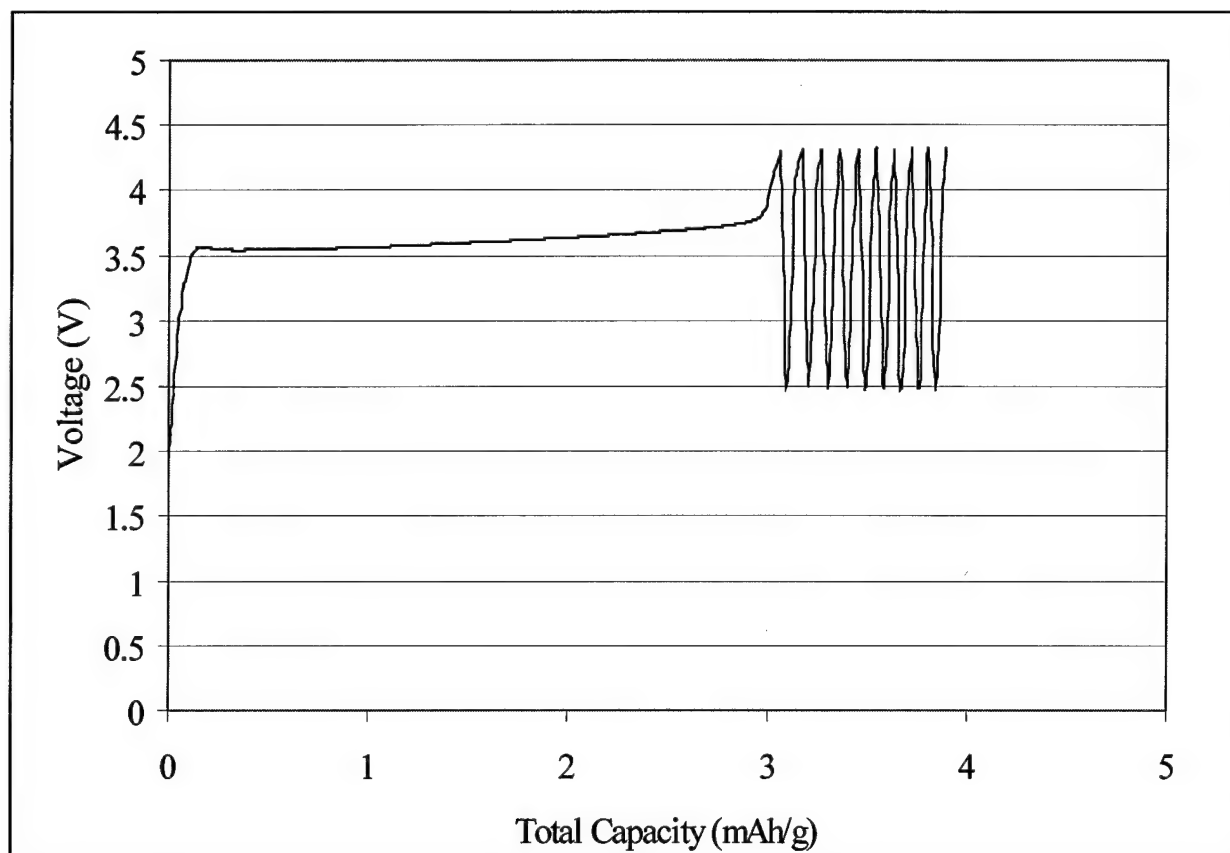


**Figure 4.11** Cycling of undoped  $\text{LiFePO}_4$  vs. Li in a stainless steel screw-top electrochemical cell using Celgard separator. 10 wt% PVdF was used as a binder in the cathode. No carbon additive was used.

The cell in Figure 4.10 was cycled again at elevated temperature ( $50^\circ \text{C}$ ) for 4 cycles. Figure 4.12 shows the charge/discharge curves. Polarization upon discharge is observed as well as decreased capacity with each successive charge.

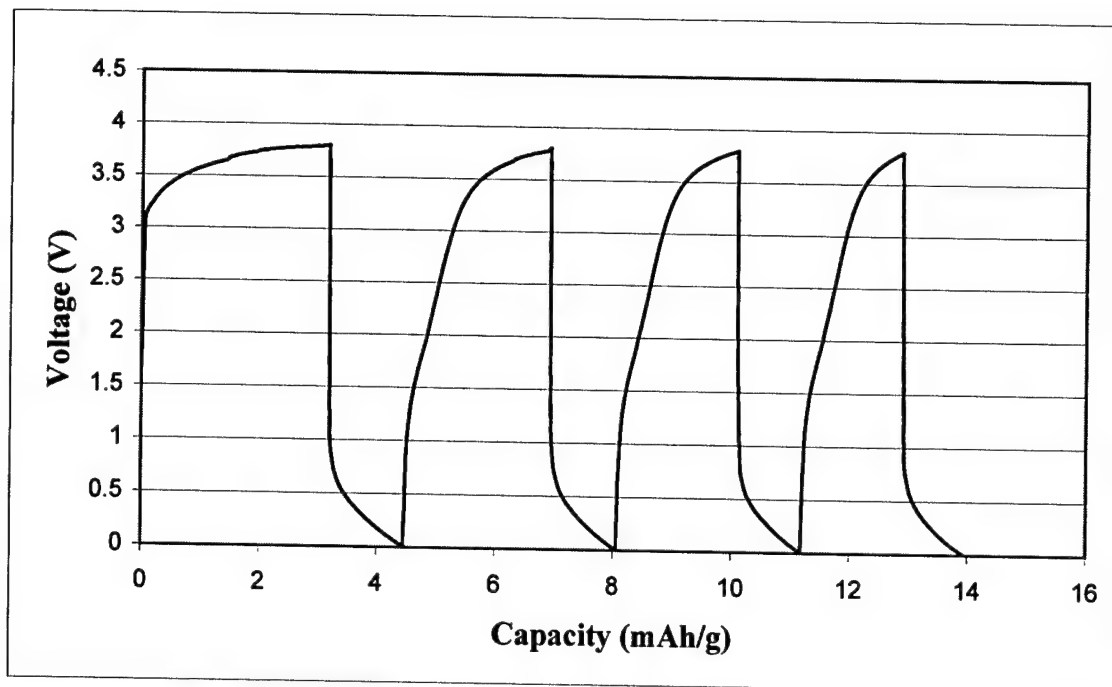


**Figure 4.12** Four charge/discharge cycles for cell of the configuration illustrated in Figure 4.8, tested at 50°C. The current rate and the capacity is calculated for LFP mass.

Finally, the cell in Figure 4.12 was charged at 5mA/g to 3.8 Volts at 50° C and removed from the battery tester. Figure 4.13 shows the resulting OCV that was recorded over time. It appeared that the cell was asymptotically approaching an equilibrium voltage just below 1 V.

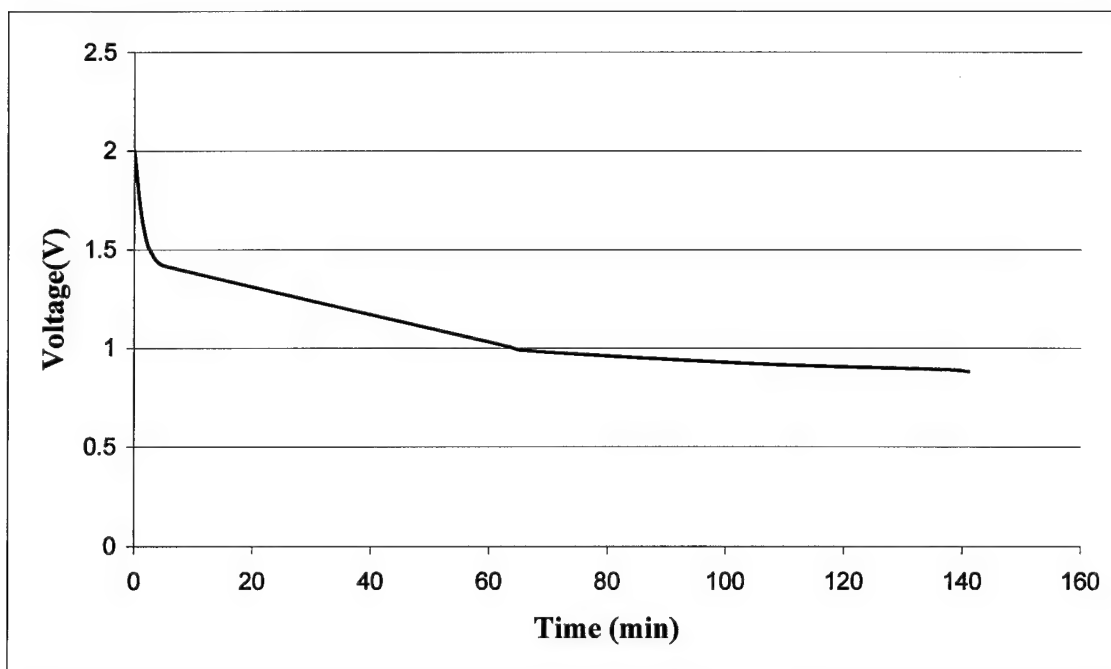


**Figure 4.13** OCV measurements for a cell after charging to 3.8 volts.

At 140 minutes after the current was set to zero, the cell had an OCV of 0.8 V. Thus, it appears that this cell is capable of holding charge.

#### **4.7 Conclusions of Electronic Isolation Experiments**

Additional interfacial resistances between two electronically conductive species consistent with  $A_{123} > 0$  have been realized experimentally. Furthermore, voltages upon charging were observed for SBS cells thermodynamically consistent with the active materials (cathode and anode) utilized. However, unless a cell exhibits discharge, other side reactions that could potentially produce similar charge curves will need to be considered. It is unclear at this time why the cells fail to show a significant discharge capacity.

#### 4.8 References

- 4-1. C.R. Yang et al. *Journal of Power Sources*, **62**, 89-93 (1996)
- 4-2. S. Neves, C.P. Fonseca, *Journal of Power Sources*, **107**, 13-17 (2002)
- 4-3. <http://www.hbcnetbase.com/hbcnet/Toc.jsp?SpaceID=10093&BookID=34&NodeID=109243040#node109243040>
- 4-4. <http://www.hbcnetbase.com/hbcnet/Toc.jsp?SpaceID=10093&BookID=34&NodeID=109243037#node109243037>
- 4-5. Cycling data of undoped  $\text{LiFePO}_4$  is provided courtesy of Jason Bloking.

## CHAPTER 5. Self-Organized Cells Using Colloidal Particle Cathode and Anodes.

Multiple experiments were performed with the purpose of producing the configuration that was proposed in Figure 2.1. In comparison to the layered geometries of Chapter 4, Self-Organized Battery System (SBS) cells using a single cast suspension containing cathode, anode, solvent, and binder were prepared and tested. The conductive olivine  $\text{Li}(\text{M}_x\text{Fe}_{1-x})\text{PO}_4$  with  $\text{M}=\text{Zr}$  and  $\text{Ti}$  was used as the cathode. MCMB served as the anode, and poly(styrene) as a binder.

### 5.1 MCMB-PS/DIM-Conductive LFP Printed Onto POMA/PVdF Substrates

Cells with the configuration in Figure 5.1 were attempted. These are expected to self-organize due to the simultaneous presence of both attractive and repulsive London dispersion forces, as described in Chapter 2.

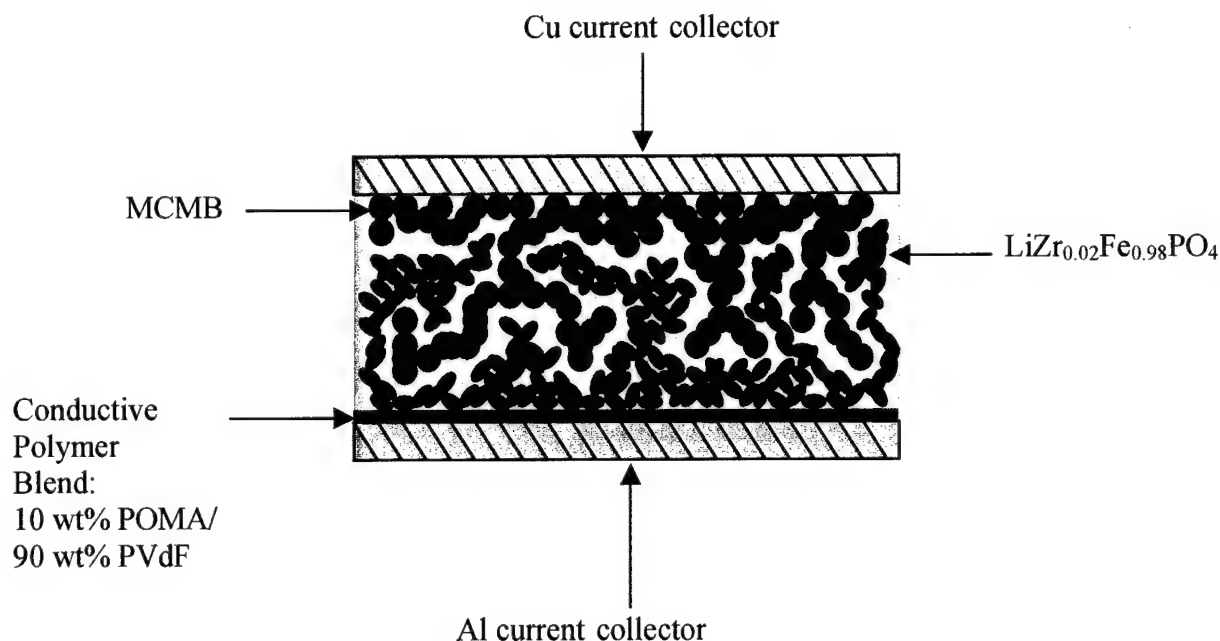


**Figure 5.1** Cell configuration of full SBS cells using 50 vol% active material  $\{\text{Li}(\text{Zr}_{0.02}\text{Fe}_{0.98})\text{PO}_4$  and MCMB $\}$ /50 vol% PS (50,000 M.W.) cast onto POMA/PVdF substrates.



Due to the low Zr dopant level, the refractive index of  $\text{LiZr}_{0.02}\text{Fe}_{0.98}\text{PO}_4$  was assumed to be the same as that of the  $\text{Li}(\text{Fe},\text{Mn})\text{PO}_4$  mineral, which has a value of  $n=1.69$ . This is below the value of DIM ( $n=1.7411$ ), so a negative  $A_{123}$  is expected between  $\text{LiZr}_{0.02}\text{Fe}_{0.98}\text{PO}_4$  and MCMB with DIM as the intervening medium. A bipolar electrochemical junction should be established in the SBS cell based upon repulsive London dispersion forces using equations 2.4 and 2.5.  $A_{123}<0$  is also expected between the Cu foil, which has  $n>2$ , and  $\text{LiZr}_{0.02}\text{Fe}_{0.98}\text{PO}_4$  when DIM is the intervening medium. This should prevent the  $\text{LiZr}_{0.02}\text{Fe}_{0.98}\text{PO}_4$  from electrically shorting between the Cu anode current collector and the POMA/PVdF conductive polymer blend at the cathode current collector. MCMB, with a refractive index of 2.5, is expected to electrically short to the Cu foil when DIM is the intervening medium, but should be repelled from the POMA/PVdF conductive polymer blend. Therefore, the MCMB should not electrically short between the two current collectors.

### 5.1.1 Experimental

100  $\mu\text{m}$  thick Al foil (Puratronic Grade Alfa-Aesar) was punched into 3/8ths inch diameter disks and coated with 10 wt% POMA/90 wt% PVdF (TFA Doped) using the techniques described in Chapter 3. The relative amounts of  $\text{Li}(\text{Zr}_{0.02}\text{Fe}_{0.98})\text{PO}_4$  and MCMB were calculated assuming a charge-balanced cell having a practical capacity of 140 mAh/g for  $\text{Li}(\text{M}_{0.02}\text{Fe}_{0.98})\text{PO}_4$  and 372 mAh/g for MCMB. An equivalent volume of PS to the volume of active materials was used. The solvent for poly(styrene) (PS), diiodomethane (DIM), was 90 vol% of the total volume of polymer and solvent. Both the  $\text{Li}(\text{Zr}_{0.02}\text{Fe}_{0.98})\text{PO}_4$  and the MCMB were dispersed in separate solvent-binder solutions, and the two were then combined to obtain the final suspension. Once  $\text{Li}(\text{Zr}_{0.02}\text{Fe}_{0.98})\text{PO}_4$ , MCMB, and the PS were mixed in DIM, the system was heated to 70° C for 20 minutes

whereupon complete dissolution of the PS occurred. After dissolution and while still hot, the SBS suspension was immediately pipetted onto aluminum substrates coated with 10 wt% POMA/90 wt% PVdF conductive blend. A copper disk was applied to the top of the wet suspension to serve as the anode current collector. All samples were dried at room temperature under vacuum for 12 hours. Upon removal from vacuum [Figures 5.2 (a) and (b)], the cells were immediately transferred to the argon filled glovebox. The cells were placed in a stainless steel screw-top electrochemical cell and 10 drops of LP 30 electrolyte (1:1 EC:DMC, 1 M LiPF<sub>6</sub>) was added. The electrochemical cells were tested with hardware provided by National Instruments and a LabVIEW operating system.

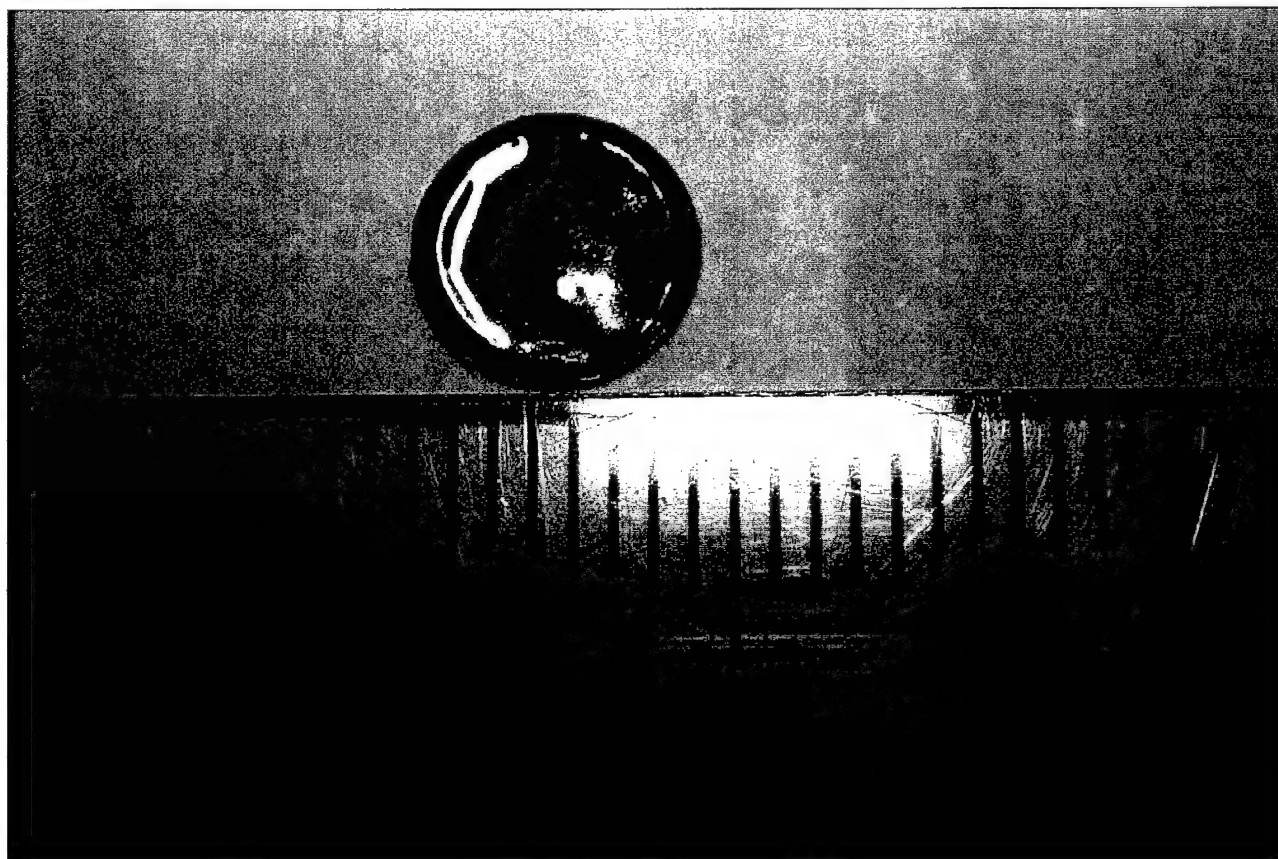


**Figure 5.2 a** Photograph of cell upon removal from vacuum at room temperature before transfer to argon filled glovebox.

DEPARTMENT OF MATERIALS SCIENCE AND ENGINEERING  
MASSACHUSETTS INSTITUTE OF TECHNOLOGY  
CAMBRIDGE, MASSACHUSETTS 02139

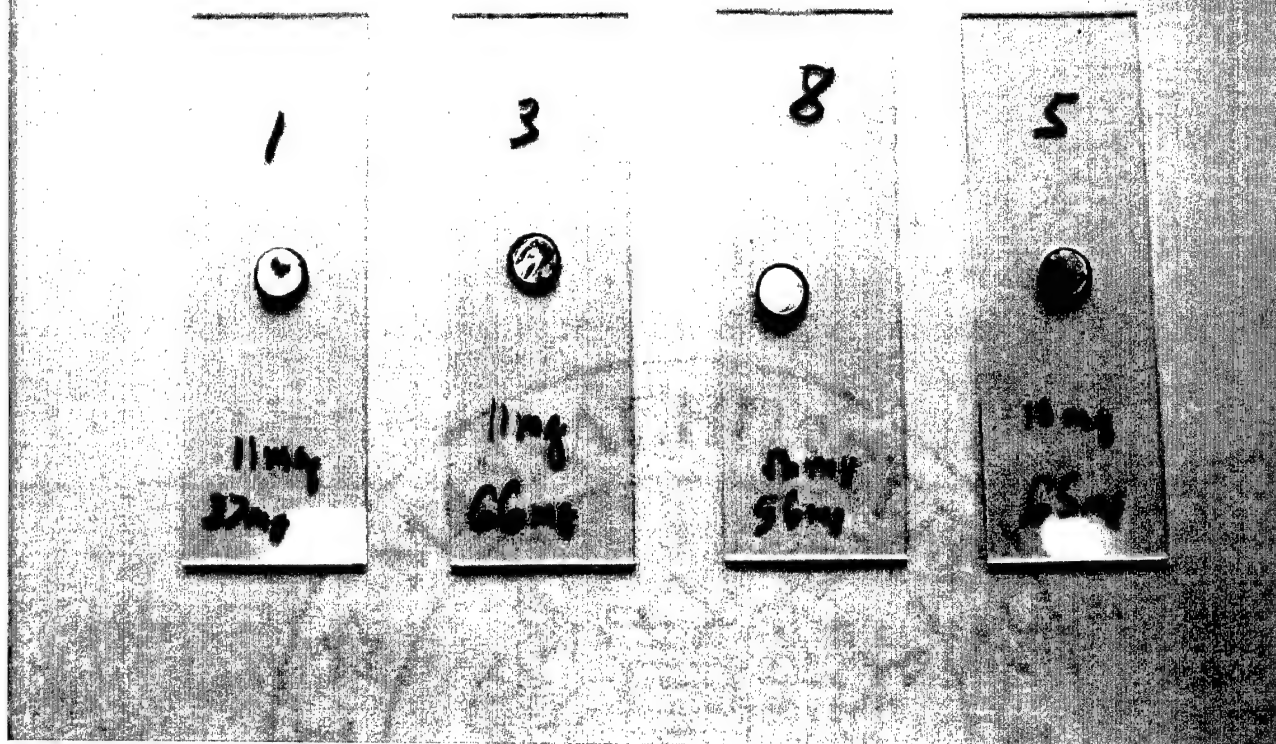
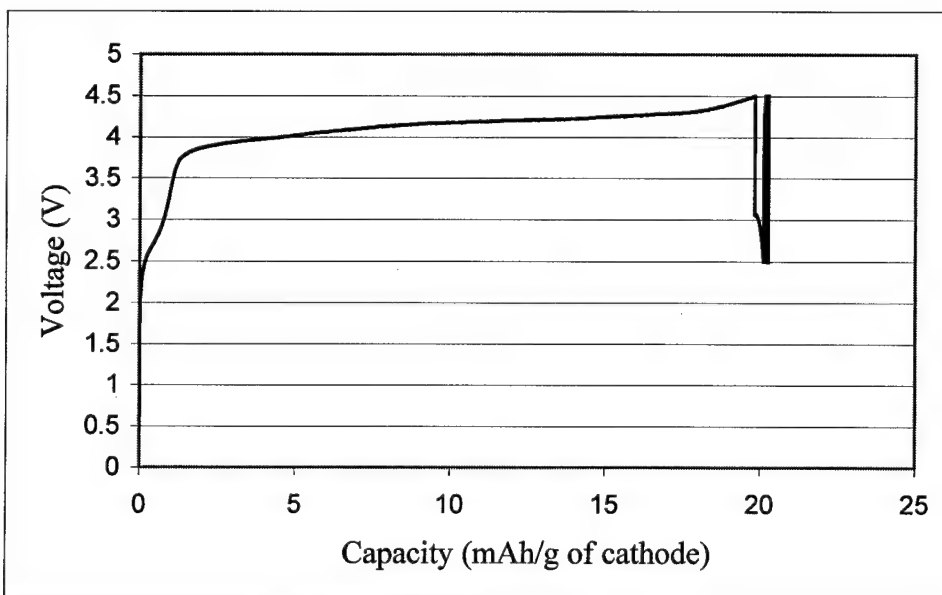


Figure 5.2 b Photograph of cells upon removal from vacuum at room temperature before transfer to argon filled glovebox.

### 5.1.2 Observations

Figure 5.3 is a charge curve obtained at a current rate of 2mA/g, calculated from the LFP mass. Figure 5.4 is an expanded view of the capacity curve around 20 mAh/g. The capacity is determined based only upon the weight of the cathode. The cell had an open circuit voltage (OCV) of 155 mV after being wet with LP 30 electrolyte and assembled in an electrochemical cell.



**Figure 5.3** Charge/discharge curves for 4 cycles, with an upper voltage cut-off of 4.5 V and lower cut-off of 2.5 V (Cell PS 210).

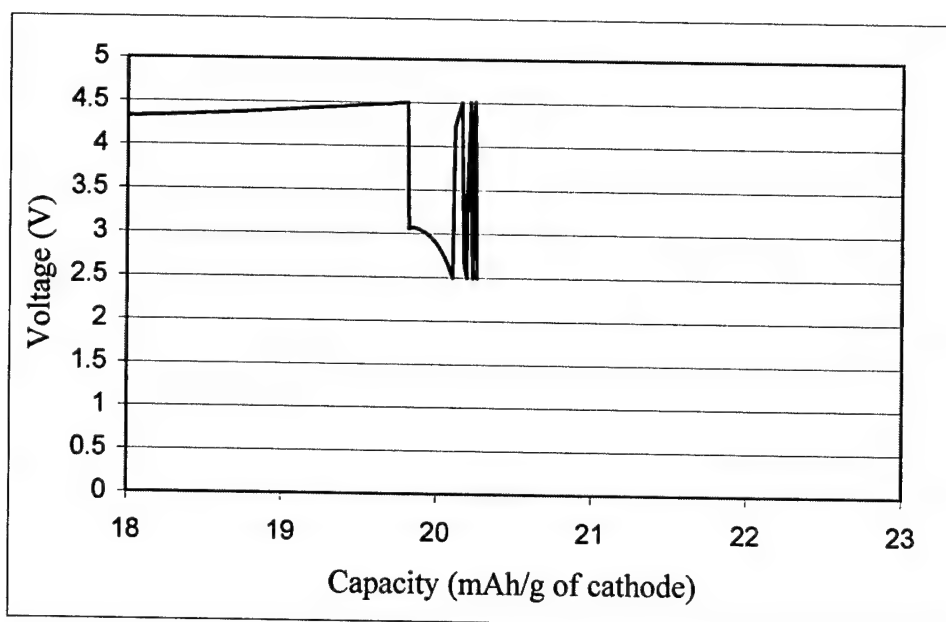


**Figure 5.4** Expanded view of the capacity curve around 20 mAh/g of Figure 5.3.

In Figure 5.3, the voltage plateau at 4 V and the voltage up turn at 20 mAh/g are indicators of cell charging. The first discharge of the cell showed a small discharge capacity starting at 3 V. To further differentiate the charging of the cell from polarization of the electrodes, the same cell was charged to 4.5 V and the OCV was measured over time (Figure 5.5). The OCV remained over 3.4 V for 3 hours before decaying slowly over 20 hours to about 1 V.

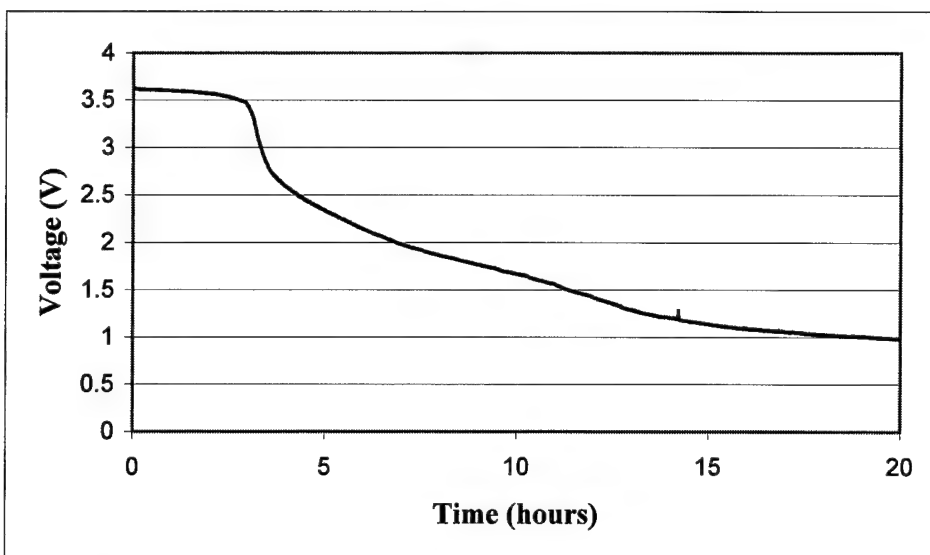


**Figure 5.5** Monitoring OCV of SBS cell (Cell PS 210).

The same cell was set to cycle again under the same conditions; however, the upper voltage limit was set to 4.3 V to prevent possible decomposition of the liquid electrolyte.

Figure 5.6 shows the respective cycling curve.

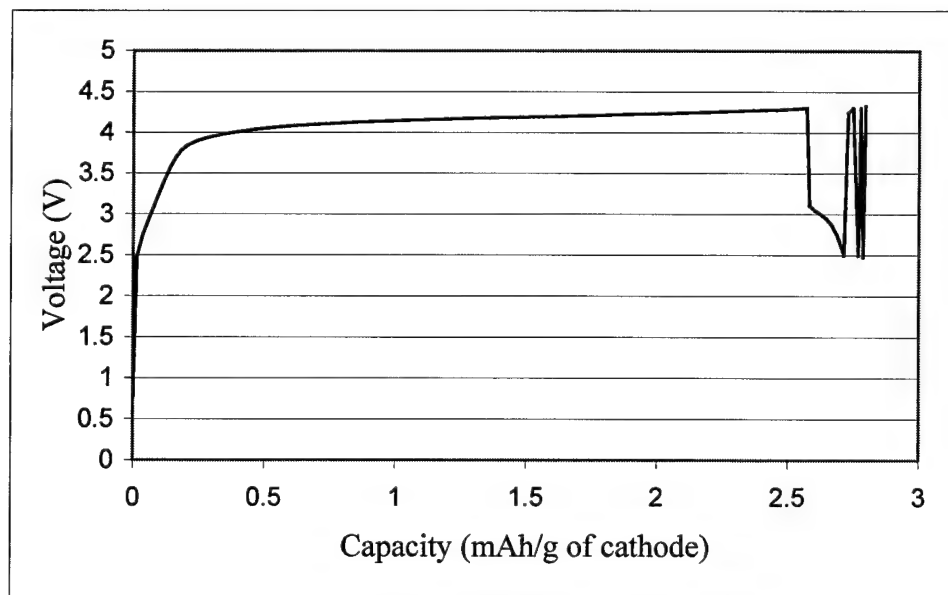


**Figure 5.6** Second cycling of SBS cell (Cell PS 210).

From Figure 5.6, a capacity of only 2.5 mAh/g was realized during the charge cycle with an upper voltage limit of 4.3 V. A small discharge capacity is again observed at 3 V. The voltage plateau at 4 V in Figure 5.6 is almost identical to that observed in Figure 5.3.

### 5.1.3 Discussion

Thermodynamically, delithiation of LFP should occur at 3.25 V vs. MCMB. Thus, it appears that delithiation of LFP with intercalation in MCMB is occurring, as well as some polarization. However, it seems that the charging is irreversible. When the cell was first charged, a capacity of 20 mAh/g was realized, which is still only 14% of the practical capacity available from  $\text{Li}(\text{Zr}_{0.02}\text{Fe}_{0.98})\text{PO}_4$  (140 mAh/g). It is possible that only the  $\text{Li}(\text{Zr}_{0.02}\text{Fe}_{0.98})\text{PO}_4$  particles that were in direct contact to the polymer film were able to be delithiated, as  $\text{Li}(\text{Zr}_{0.02}\text{Fe}_{0.98})\text{PO}_4$  may not provide sufficient electronic conductivity through the particle-particle contacts depicted in Figure 5.1. Upon subsequent cycling, the cell did not charge further. Nonetheless, the cell held an OCV of over 3.4 V for 3 hours (Figure 5.5).

Another possibility is that the refractive index of  $\text{Li}(\text{Zr}_{0.02}\text{Fe}_{0.98})\text{PO}_4$  is greater than that of the intervening medium, DIM. If the refractive index is higher than the 1.69 that was assumed, then both the  $\text{Li}(\text{Zr}_{0.02}\text{Fe}_{0.98})\text{PO}_4$  and the MCMB would be repelled from the surface of the POMA/PVdF conductive blend. In this instance, the charging behavior observed could be that for the POMA cycling as a cathode against the MCMB. It is known that POMA is electrochemically active as a cathode material, with a voltage plateau from 3 to 3.8 V relative to a lithium metal anode. The protonic doping mechanism for POMA is a competitive process to the charge-storage mechanism when POMA is used as a cathode. Upon charging, oxidation of the nitrogen on the polymer backbone is charged balanced by the Li-salt anion, which releases the Li ion for

intercalation into the anode. This charge storage mechanism provides POMA with a practical capacity of 95 mAh/g. However, the low level of POMA (approximately 0.1 mg) that is present in the conductive polymer blend, and the high level of TFA doping, should provide negligible capacity when the present POMA/PVdF blends are cycled against MCMB—clearly not enough to provide the capacity observed in Figure 5.3. For the POMA that is present, assuming that it is at least 50% doped with TFA, a maximum capacity of 5 mAh/g could be realized, which is only one-fourth of the observed charge capacity.

## **5.2 Self-Organized MCMB-PS/DIM-Conductive LFP on POMA/PVdF Substrates, Cycled in a Pressure Free Cell**

The pressure applied to the sample in the stainless steel screw-top electrochemical cell is not precisely known. A positive Hamaker constant and an attractive force exist between  $\text{Li}(\text{Zr}_{0.02}\text{Fe}_{0.98})\text{PO}_4$  and MCMB when liquid electrolyte (LP 30) is the intervening medium in the assembled cell. After conducting the experiments in section 5.1, it was speculated that possibly the pressure applied to the sample upon assembly of the cell was causing the cell to electronically short since the repulsive interaction is now replaced with an attractive interaction. Thus, experiments were conducted where no direct pressure was placed on the sample during cycling.

### **5.2.1 Experimental**

100  $\mu\text{m}$  thick Al foil (Puratronic Grade Alfa-Aesar) was punched into 3/8ths inch diameter disks and coated with 10 wt% POMA/90 wt% PVdF (TFA Doped) using the techniques described in Chapter 3. The relative amounts of  $\text{Li}(\text{Zr}_{0.02}\text{Fe}_{0.98})\text{PO}_4$  and MCMB were calculated assuming a charge balanced cell having a practical capacity of 140 mAh/g for  $\text{Li}(\text{M}_{0.02}\text{Fe}_{0.98})\text{PO}_4$  and 372 mAh/g for MCMB. An equivalent volume of



PS to the volume of active materials present was used. The solvent for poly(styrene) (PS), diiodomethane (DIM), was 90 vol% of the total volume of polymer and solvent. Both the  $\text{Li}(\text{Zr}_{0.02}\text{Fe}_{0.98})\text{PO}_4$  and the MCMB were dispersed in separate solvent-binder solutions, and the two were then combined to obtain the final suspension. Once  $\text{Li}(\text{Zr}_{0.02}\text{Fe}_{0.98})\text{PO}_4$ , MCMB, and the PS were mixed in DIM, the system was heated to 70°C for 20 minutes where upon complete dissolution of the PS occurred. After dissolution and while still hot, the SBS suspension was immediately pipetted onto aluminum substrates coated with 10 wt% POMA/90 wt% PVdF conductive blend. A copper disk with a copper lead was applied to the top of the wet suspension to serve as the anode current collector. All samples were dried at room temperature under vacuum for 12 hours. Upon removal from vacuum, the cells were immediately transferred to the argon filled glovebox. The cells were placed in a stainless steel electrochemical cell and 10 drops of LP 30 electrolyte (1:1 EC:DMC, 1 M  $\text{LiPF}_6$ ) was added. Figure 5.7 shows how the pressure-free cells were assembled. The Cu lead was bent orthogonal to the cell and inserted into the Teflon lined base of the stainless steel electrochemical cell. 10 drops of LP 30 electrolyte was used. Due to the open cell configuration, Teflon tape was used on the threads of the screw-top glass jar and black plastic electrical tape sealed the lid on the outside to prevent loss of the argon atmosphere inside the jar. The electrochemical cells were tested with hardware provided by National Instruments and a LabVIEW operating system.

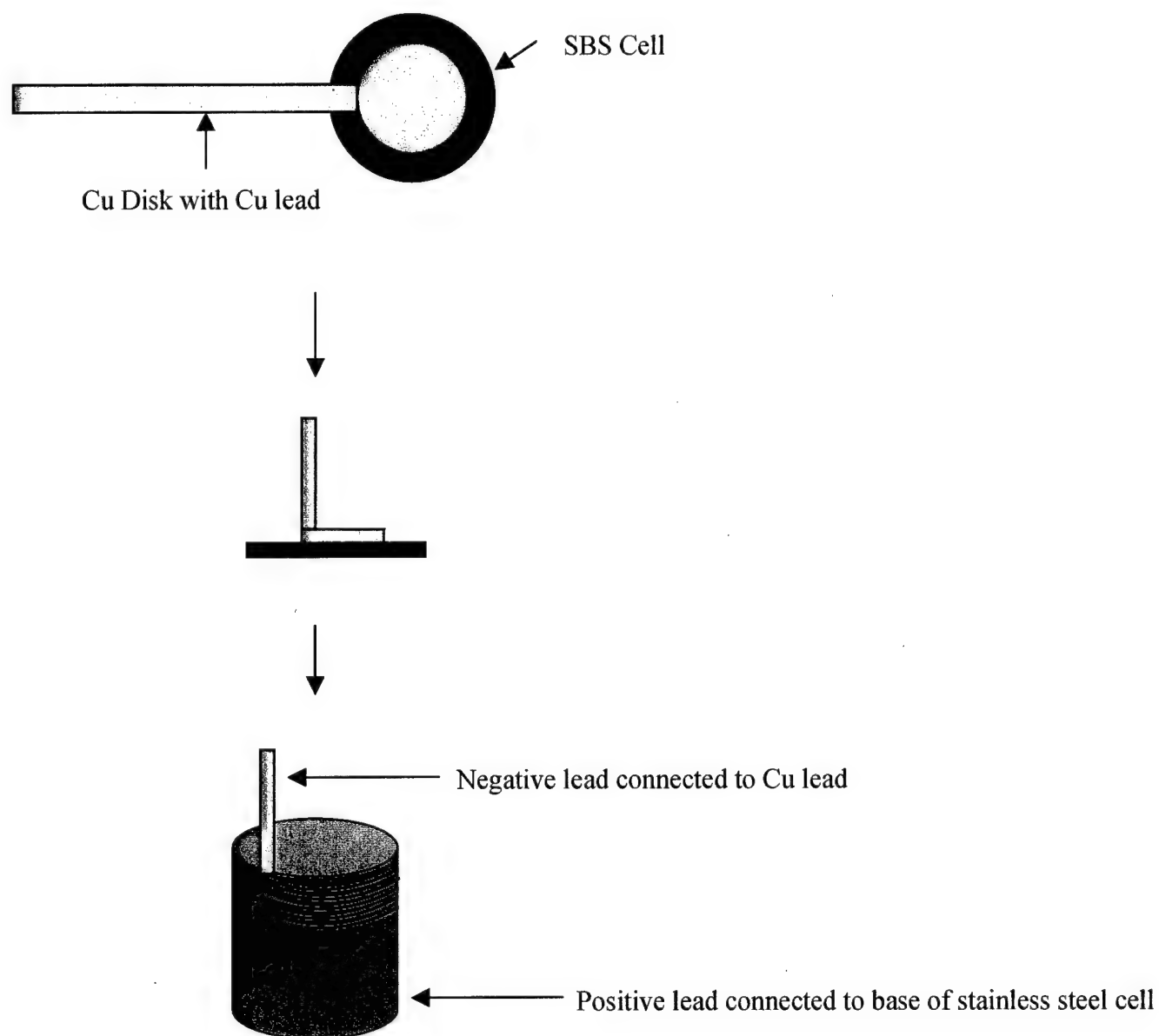


**Figure 5.7** Pressure-free electrochemical cell assembly.

### 5.2.2 Observations

The charge curve in Figure 5.8 was obtained at a current rate of 2 mA/g, calculated from the mass of LFP. The voltage plateau at 3.8 V upon charging is consistent with LFP cycled against MCMB, plus  $\sim 0.5$  V of polarization. At a capacity of 6 mAh/g (after 18 hours of charging), the current was turned off and the OCV was monitored over time. The cell maintained an OCV of 3.6 V for 21 hours (Figure 5.9). At that point, a malfunction caused the battery tester to spontaneously charge the cell up to the upper voltage limit of 4.3 V, and discharge to the lower voltage limit of 2.5 V. Thereafter, the cell would no longer hold a voltage above about 1.8 V, suggesting that internal shorting was occurring (Figure 5.10). In Figure 5.10, all the data was collected while the battery tester was in charge mode. However, at the completion of testing, the cell still had an OCV of 380 mV and an internal cell resistance of  $4.74\text{ M}\Omega$ , indicating that electrical isolation was still present.

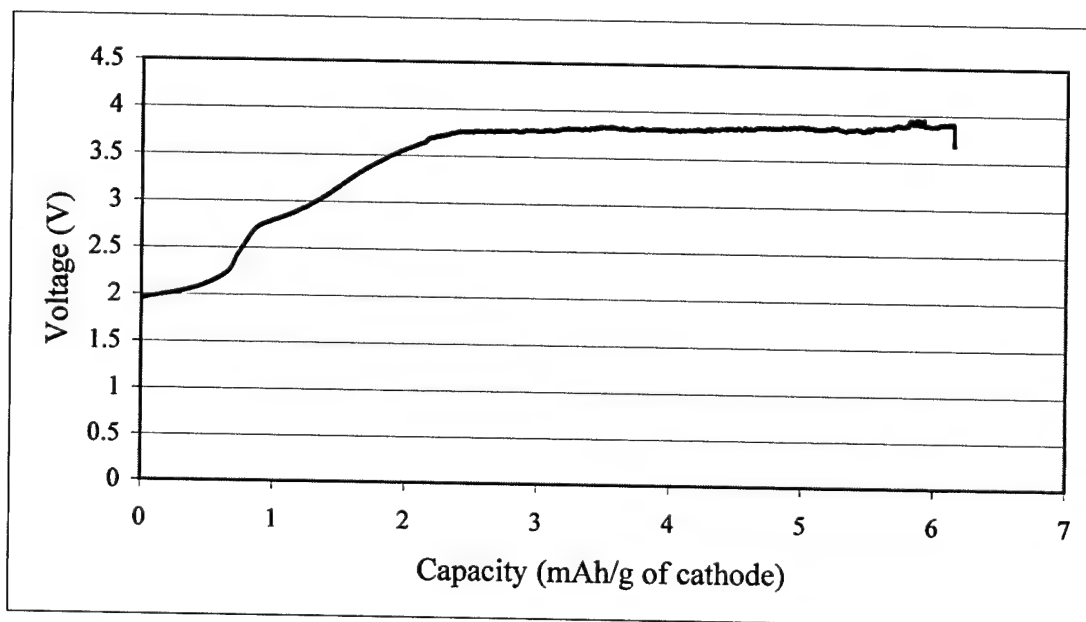


**Figure 5.8** Charging of SBS cell with pressure-free configuration (PS 215).

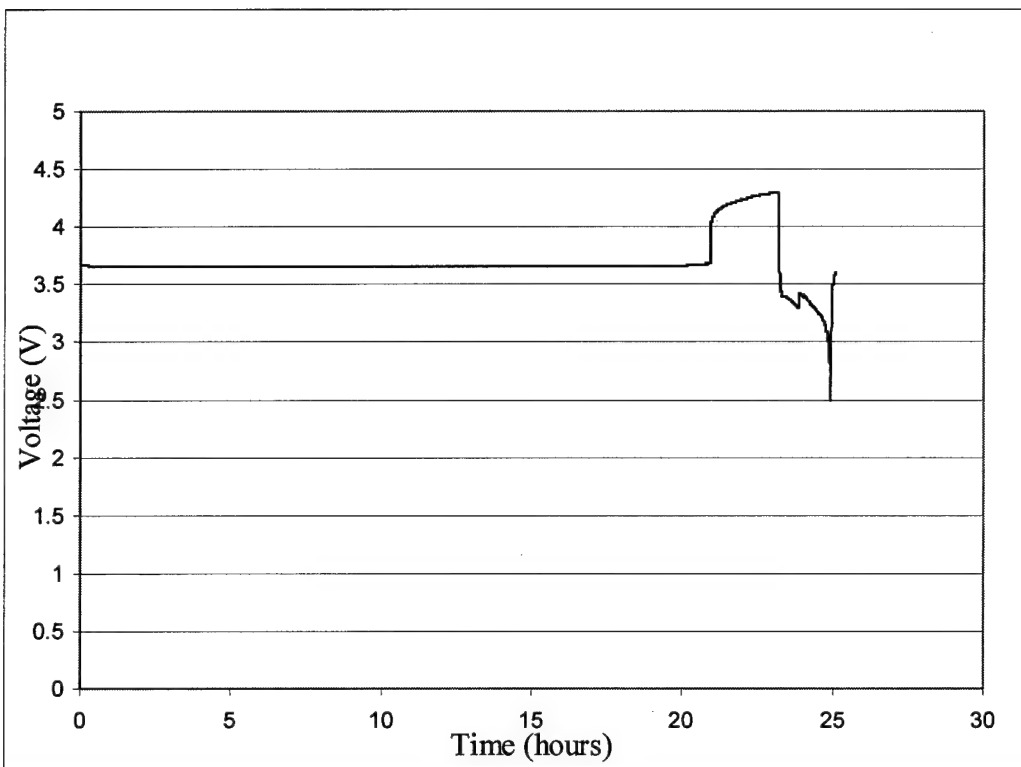


**Figure 5.9** OCV of SBS cell PS 215, showing that an OCV of 3.6 V is held for over 20 hours.

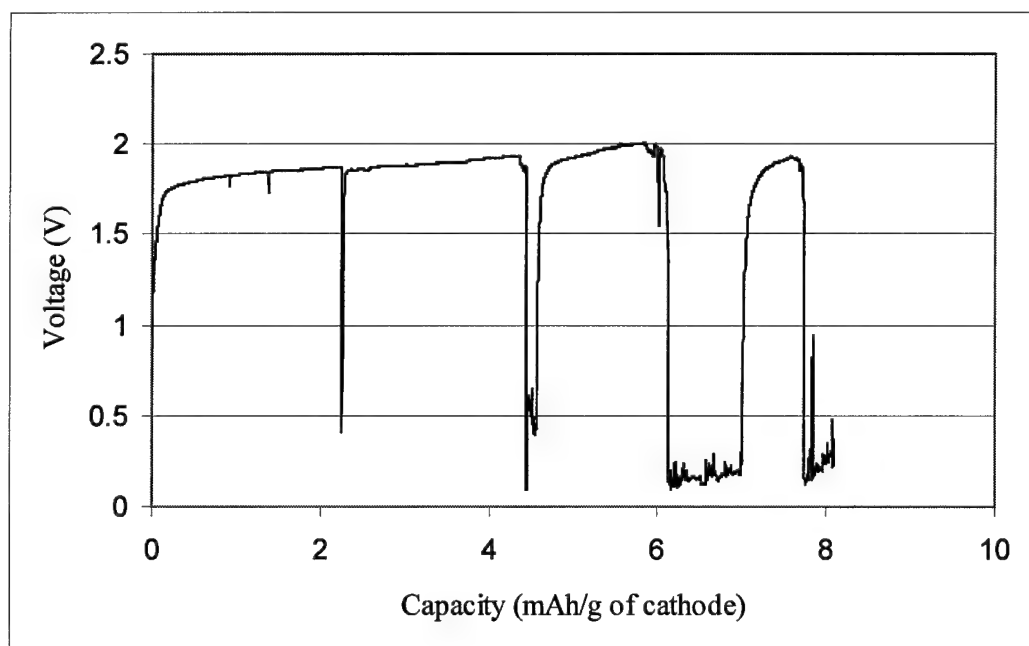


**Figure 5.10** Charge data of cell PS215 after holding 3.6 volts for over 20 hours.

### 5.2.3 Conclusions

From these test results, it appears that charging of the  $\text{Li}(\text{Zr}_{0.02}\text{Fe}_{0.98})\text{PO}_4$  was taking place. The delithiation voltage at 3.8 V observed for the LFP cycled against MCMB is consistent with a charging plateau with slight polarization. The 0.1 mg of POMA (capacity of 95 mAh/g) that is present would provide less than 1 mAh/g of observed capacity in Figure 5.8. Therefore, it is concluded that the capacity observed in Figure 5.8 is due to the charging of the LFP.

### 5.3 Self-Organized MCMB-PS/DIM-Conductive LFP Suspensions on POMA/PVdF Substrates: Effect of PS Fraction and Phase Purity of LFP Powder

After conducting the experiments in sections 5.1 and 5.2, it was determined that the  $\text{Li}(\text{Zr}_{0.02}\text{Fe}_{0.98})\text{PO}_4$  used in the experiment may have had an  $\text{Fe}_2\text{P}$  second phase present as well as a small percent (2-5 wt%) of carbon. The carbon could allow for electronic shorting between the  $\text{Li}(\text{Zr}_{0.02}\text{Fe}_{0.98})\text{PO}_4$  and the MCMB. It is uncertain what effect the  $\text{Fe}_2\text{P}$  could have had on the cycling performance. A new cathode powder,  $\text{Li}(\text{Ti}_{0.02}\text{Fe}_{0.98})\text{PO}_4$ , was processed and verified to be single-phase, and to have electronic conductivity  $>10^{-3}$  S/cm at room temperature. In addition, the vol% of PS was increased from that used in section 5.2 to further prevent shorting between  $\text{Li}(\text{Ti}_{0.02}\text{Fe}_{0.98})\text{PO}_4$  and MCMB once the DIM was removed and the liquid electrolyte was added to the cell for cycling.

#### 5.3.1 Experimental

100  $\mu\text{m}$  thick Al foil (Puratronic Grade Alfa-Aesar) was punched into 3/8ths inch diameter disks and coated with 10 wt% POMA/90 wt% PVdF (TFA Doped) using the techniques described in Chapter 3. The relative amounts of  $\text{Li}(\text{Ti}_{0.02}\text{Fe}_{0.98})\text{PO}_4$  and MCMB were calculated assuming a charge-balanced cell having a practical capacity of

140 mAh/g for  $\text{Li}(\text{Ti}_{0.02}\text{Fe}_{0.98})\text{PO}_4$  and 372 mAh/g for MCMB. 60 vol% of PS was used based upon the total volume of polymer and active materials present. The solvent for poly(styrene) (PS), diiodomethane (DIM), was 90 vol% of the total volume of polymer and solvent. Both the  $\text{Li}(\text{Ti}_{0.02}\text{Fe}_{0.98})\text{PO}_4$  and the MCMB were dispersed in separate solvent-binder solutions, and the two were then combined to obtain the final suspension. Once  $\text{Li}(\text{Ti}_{0.02}\text{Fe}_{0.98})\text{PO}_4$ , MCMB, and the PS were mixed in DIM, the system was heated to 70° C for 20 minutes where upon complete dissolution of the PS occurred. After dissolution and while still hot, the SBS suspension was immediately pipetted onto aluminum substrates coated with 10 wt% POMA/90 wt% PVdF conductive blend. A copper disk was applied to the top of the wet suspension to serve as the anode current collector. All samples were dried at room temperature under vacuum for 12 hours. Upon removal from vacuum, the cells were immediately transferred to the argon filled glovebox. The cells were placed in a stainless steel screw-top electrochemical cell and 10 drops of LP 30 electrolyte (1:1 EC:DMC, 1 M  $\text{LiPF}_6$ ) was added. The electrochemical cells were tested with hardware provided by National Instruments and a LabVIEW operating system.

### 5.3.2 Observations

Upon assembling in the stainless steel electrochemical cell and adding the liquid electrolyte, the cell had an OCV of 90 mV and internal cell resistance 0.8 M $\Omega$ . The charge curve obtained in Figure 5.11 was obtained at a charging current of 5 mA/g, calculated from the LFP mass. A capacity of 80 mAh/g in the first charge was calculated from the weight of cathode present. The voltage plateau from 3.2 to 3.7 V in Figure 5.11 is consistent with  $\text{Li}(\text{Ti}_{0.02}\text{Fe}_{0.98})\text{PO}_4$  cycled against MCMB. Negligible discharge

capacity was observed to a lower voltage limit of 2.5 V. After the data collection in Figure 5.11 was complete, the cell was restarted 7 hours later with a charging current of 5 mA/g, a discharge current of 20 mA/g, a lower voltage limit of 0.5 V, and an upper voltage limit of 4.3 V (Figure 5.12). A capacity of 8 mAh/g was realized, with a voltage plateau that is again consistent with  $\text{Li}(\text{Ti}_{0.02}\text{Fe}_{0.98})\text{PO}_4$  cycled against MCMB. A small discharge capacity under high polarization was observed. Upon completion of testing, the cell had an OCV of 103 mV and an internal cell resistance  $0.8 \text{ M}\Omega$ .

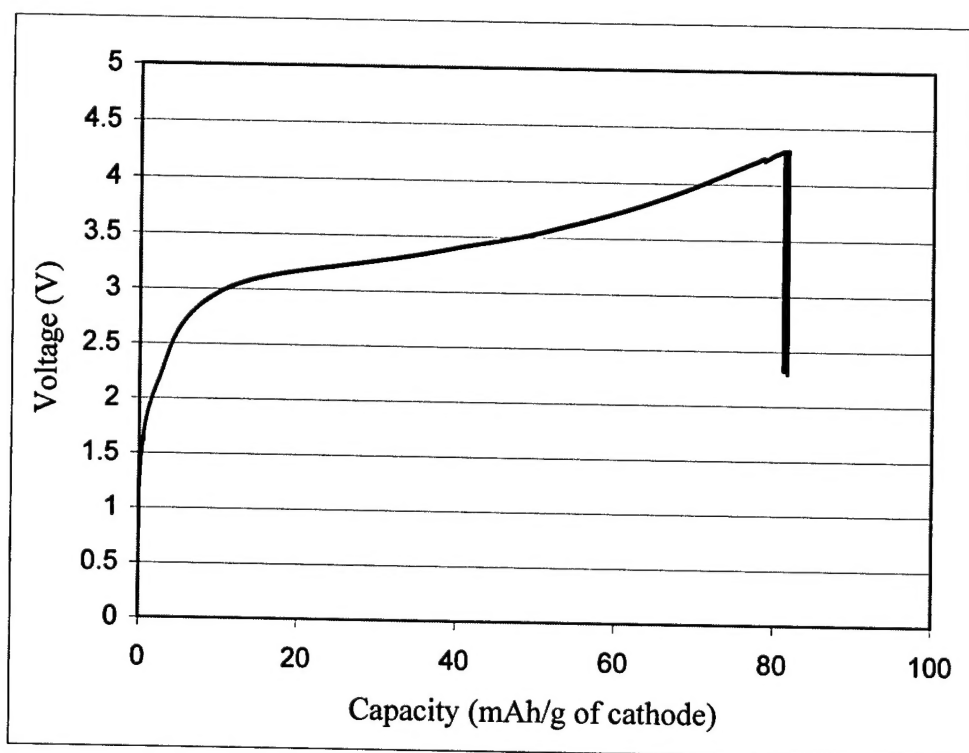


**Figure 5.11**  $\text{LiTi}_{0.02}\text{Fe}_{0.98}\text{PO}_4$  cycled against MCMB in a self-organized system (Cell PS 233).

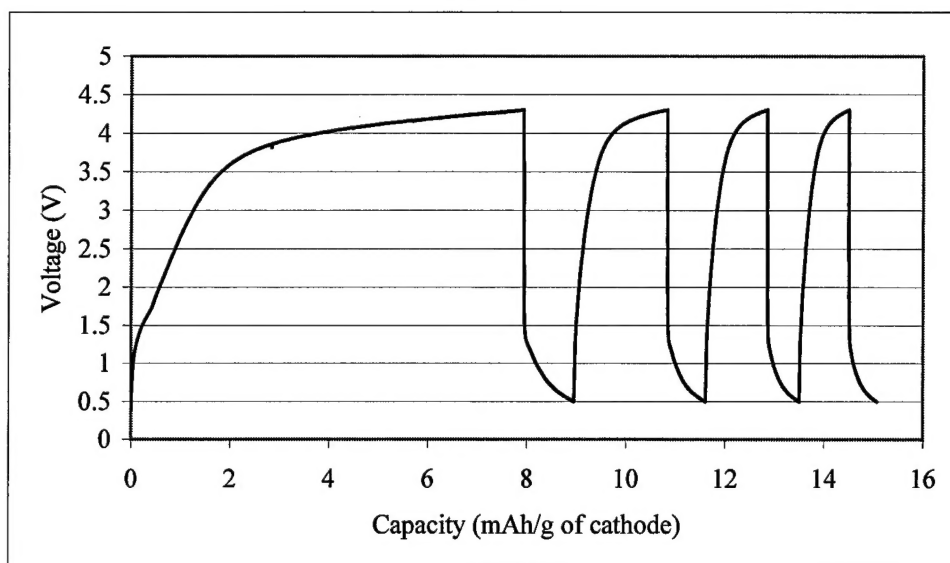


**Figure 5.12** Data collected 7 hours after first data set collected (Figure 5.11). First charge shows a capacity of only 8 mAh/g compared to 80 mAh/g in the first charge curve of Figure 5.11 (Cell PS 233).

### 5.3.3 Conclusions

The large charge capacity realized in Figure 5.11 of 80 mAh/g further supports the charging of the  $\text{Li}(\text{Ti}_{0.02}\text{Fe}_{0.98})\text{PO}_4$  as the cause of the capacity observed in the charge curves. Although side reactions must always be considered in electrochemical tests, the smooth profile observed in Figures 5.11 and 5.12 suggests a charging mechanism rather than a side reaction such as corrosion.



## CHAPTER 6. Conclusions

This thesis presents new concepts for self-organized electrochemical devices, and describes experiments conducted to test the feasibility of the concepts as applied to the specific example of a lithium rechargeable battery. These model experiments have been conducted using individual components in the self-organized battery system that are known and have been extensively characterized by previous researchers. Specifically, all of the cathode, anode, and liquid electrolyte materials utilized have been proven in Li ion cells. Furthermore, the SBS cells have been investigated using electrochemical tests that are widely applied to conventional battery systems.

A conductive polymer blend was established that can serve as a low refractive index end member of a self-organized battery. This material, applied as particle coatings, deserves further attention as a method of obtaining low refractive index, electronically and ionically conductive materials for one component of the SBS cell. Electronic isolation is clearly observed between POMA/PVdF polymer blend and MCMB when DIM is the intervening medium and PEO is the binder, consistent with a negative Hamaker constant. Similarly, additional interfacial resistances are observed between LMCO and a POMA/PAN polymer blend when DIM is the intervening medium. Here, LMCO is the high refractive index material.

In the absence of the low refractive index polymer films, reliable electronic isolation is observed between doped LFP/PVdF composite films and MCMB/PS when DIE is the intervening medium. In each instance, the additional resistance observed is consistent with an expected negative  $A_{123}$ . Furthermore, the cycling of doped LFP vs. MCMB in the layered configuration showed a cell voltage consistent with thermodynamic

intercalation between the cathode and anode materials used. However, it is unclear at this time why the cells fail to show a significant discharge capacity.

In the fully interpenetrating SBS cells made using a single suspension containing particles of both cathode and anode, it appears that charging of the doped LFP was taking place. The delithiation voltage at 3.8 V observed for the LFP cycled against MCMB is consistent with the expected charging voltage plus a slight polarization. Moreover, the substantial charge capacity of 80 mAh/g observed further supports the charging of the cathode as the cause of the capacity observed in the charge curves. Although side reactions must always be considered in electrochemical tests, the smooth profiles observed suggests a charging mechanism rather than a side reaction such as corrosion.

Thus, the feasibility has been demonstrated in several experimental geometries for the key concept of electrical isolation of conductive electrode materials using repulsive dispersion forces, and the creation of an electrochemical junction. While much additional work is necessary to improve the processing and device characteristics, these results pave the way for subsequent studies that may lead to commercialization.